



Project Report

Optimal design of rubber joints for seismic protection of masonry-infilled frame structures

EEFIT Research Grant Scheme 2019
The Institution of Structural Engineers

Dr. Enrico Tubaldi

Mr. Prateek Kumar Dhir

Ms. Alessandra Orfeo

Department of Civil and Environmental Engineering
University of Strathclyde, Glasgow

Abstract

This report presents the results of an extensive experimental campaign and of numerical analyses aimed at characterising the cyclic shear behaviour of masonry triplets with mortar-rubber joints under both monotonic and cyclic loading. These joints are consisting of rubber strips placed between two mortar layers with the aim of enhancing the flexibility of masonry components while providing some auxiliary energy dissipation. The main application of the rubber joints is for enhancing the performance of masonry-infilled reinforced concrete frames under both in-plane and out-of-plane loading, thanks to a reduced interaction between the infill panels and the frame. Although past tests have investigated the behaviour of multi-layer flexible joints, no in-depth study has been carried out to date on the hysteretic and dissipative properties of mortar-rubber joints. In order to fill this gap, a series of experimental tests were conducted at the University of Strathclyde to characterise the mechanical behaviour of the various components of the rubber-masonry triplets as well as the behaviour of the composite system, with particular focus on the cyclic shear response and the bond strength. The hysteretic responses of the triplets obtained from the experiments are simulated using a finite element modelling strategy developed in Abaqus. The study results are useful for informing modelling strategies for the design and analysis of rubber joints, and for the selection of the most suitable rubber compound and layer geometrical properties.

Key Words: Masonry triplets, Monotonic shear, Cyclic shear, rubber joints, hysteretic behaviour

Contents

Abstract	2
Contents	3
List of Figures	4
List of Tables	7
1 Introduction	8
2 Experimental Campaign	11
2.1 Brick and mortar characterization	11
2.2 Characterisation of rubber joints	16
2.3 Manufacturing of masonry triplets and experimental tests set-up.....	19
2.4 Monotonic and Cyclic shear tests of triplets.....	21
3 Simulation of experimental tests	30
3.1. Simulation of experimental tests on triplets with mortar joints.....	30
3.2. Simulation of characterization rubber material tests and cyclic tests on triplets with mortar-rubber joints.....	32
4 Modelling of RC frames with infill walls and rubber joints	39
4.1. Advanced mesoscale modelling.....	39
4.2. Simplified macro-scale model	40
4.3. Case study validation	41
4.4. Model developments.....	45
5 Concluding Remarks	46
Acknowledgments	46
References	47

List of Figures

Figure 1. Masonry infilled walls with horizontal and vertical joints.

Figure 2. Rubber joints developed by TARRC (Ahmadi, Dusi and J. Gough., 2017)

Figure 3. (a) Demonstration of TARRC's rubber wall joint deployment at SAIE Bologna (SAIE, 2015) (b) Masonry infilled frame with horizontal and vertical rubber joints tested within INSYSME project (EU Project INSYSME, 2016)

Figure 4. (a, b) compressive strength test on bricks in horizontal and vertical direction (c) test setup for three-point bending test of brick specimens (d, e) failed brick specimens (f) load-displacement response of brick specimens

Figure 5. (a, b) Casting (c, d) testing (e, f) failed mortar specimens for the three-point bending test (at 28 days)

Figure 6. (a, b) Casting and preparation (c, d) testing of mortar cubes for 28-days Compressive strength tests

Figure 7. (a) Three-point bending of mortar beams (b) compression tests of mortar cubes at 28 days.

Figure 8. (a, b) tensile test setup of rubber specimen (c, d) deformed shape before and after the test (e) tensile stress- strain response (f) relaxation test.

Figure 9. (a) detailed dimension (b) test setup (c) deformed shape of the quadruplet

Figure 10. (a) Shear stress-strain response (b) relaxation test on rubber quadruplet

Figure 11. (a) Typical Birtley old English bricks used (b) rubber joints (c, d) dimensions of the triplets with mortar and mortar-rubber joints (e) triplet with mortar joint (f) triplets with mortar-rubber joints

Figure 12. (a) Shear test set-up (b) forces configuration for cyclic shear test

Figure 13. Testing equipment apparatus used to perform shearing tests on triplet specimens.

Figure 15. (a, b) Monotonic (c, d) Cyclic shear test of mortar triplets with 0.2 MPa pre-compression

Figure 16. (a, b) Monotonic (c, d) Cyclic shear test of mortar triplets with 0.4 MPa pre-compression.

Figure 17. (a, b) Monotonic (c, d) Cyclic shear test of mortar triplets with 0.6 MPa pre-compression

Figure 18. (a) Cyclic shear test setup (b) test specimens.

Figure 19. Shear response of triplets with mortar-rubber joints for various levels of pre-compressions

Figure 20. Variation of the (a) secant shear modulus (b) equivalent damping with increasing shear strain at different compression levels.

Figure 22. (a, b) Monotonic (c, d) Cyclic shear test of innovative triplets with 0.2 MPa pre-compression

Figure 23. (a, b) Monotonic (c, d) Cyclic shear test of innovative triplets with 0.4 MPa pre-compression

Figure 24. (a, b) Monotonic (c, d) Cyclic shear test of innovative triplets with 0.6 MPa pre-compression

Figure 25. Relationship between shear strength and pre-compression stress for triplets

Figure 26. (a) FE model with refined mesh (b) plastic strain distributions for mortar triplets

Figure 27. (a, b, c) Comparison of experimental and numerical response of the mortar triplets under monotonic loading at (a) 0.2 MPa (b) 0.4 MPa (c) 0.6 MPa pre-compression (d) Comparison of numerical responses only

Figure 28. Comparison of experimental and calibrated numerical response of the (a) tensile and (b) relaxation test on tensile rubber sample, (c) shear and (d) relaxation test on quadruplet rubber specimen

Figure 29. (a) FE model of the masonry triplets with mortar-rubber joints, (b) nominal strain distributions for mortar-rubber triplets

Figure 30. Comparison of experimental and numerical cyclic shear response of the masonry triplet at 10 mm amplitude and pre-compression

Figure 33. (a) Infilled frame with horizontal and vertical flexible/sliding joints and (b) mechanical scheme of a macro-element

Figure 34 Geometric details of the frame with traditional infill (dimensions in mm)

Figure 35 (a) Minimum principal compressive stress distribution (b) Plastic strain contour plots for infilled frame with rubber joints (c) Deformed shape of the DMEM for a horizontal displacement of 55mm (2.0% drift)

Figure 36. Comparison between numerical responses of the bare frame, infilled frame with traditional infills and infill with rubber joints under monotonic loading.

List of Tables

Table 1. Mechanical properties of clay brick specimens

Table 2. Mechanical properties of mortar specimens

Table 3. Peak load of masonry triplets subjected to monotonic shear tests.

Table 4. Mechanical properties of the triplet components (brick and mortar units).

Table 4. Mechanical properties of the triplet components (brick and mortar units).

Table 5. Properties of the contact interfaces describing the brick-mortar joints

Table 6 Material parameters of Yeoh model (MPa) and Bergstrom-Boyce model

Table 7. Properties of the contact interfaces describing the mortar-rubber joints

Table 8. Main mechanical properties of RC components and selected masonry infill.

Table 9. Properties of the contact interfaces describing the mortar joints

Table 10. Interaction properties of the mortar-rubber joints in the mesoscale model.

1. INTRODUCTION

Seismic events throughout the world have demonstrated the high vulnerability of masonry infills in reinforced concrete (RC) frame structures. While structural members such as columns and beams are designed to be earthquake-resistant, masonry infills are often disregarded in design calculations, since they are treated as non-structural components. For this reason, they often undergo severe damage even under minor earthquakes, which may lead to injury and death of occupants and may also hamper rescue operations. The economic losses can be considerable, with many studies (Villaverde, 1997; Filiatrault and Sullivan, 2014; Del Vecchio *et al.*, 2018; De Risi, Del Gaudio and Verderame, 2019) showing that the repair cost of infills may significantly exceed that of structural components.

In the recent years, alternative design solutions have been proposed for engineered infill walls with enhanced behaviour, exhibiting minimal interaction with the building structural components. The idea behind most of the proposed techniques is to increase the flexibility of the infill panel and to isolate it from the surrounding frame through the introduction of interlocking layers (Misir, 2015), sliding layers (Preti, Bettini and Plizzari, 2007, 2012; Bolis *et al.*, 2015, 2019; Preti, Migliorati and Giuriani, 2015; Morandi, Milanesi and Magenes, 2016, 2018; Preti *et al.*, 2016; Bolis, Stavridis and Preti, 2017; Morandi *et al.*, 2017; Preti, Bolis and Stavridis, 2019; Di Trapani *et al.*, 2020) and flexible/soft layers (Mojsilović, 2012; Anglada, 2014; Vögeli, Mojsilović and Stojadinović, 2015; Mojsilović, Petrović and Anglada, 2015; Mojsilović, Petrović and Anglada, 2015; Verlato *et al.*, 2016; Calabria *et al.*, 2016; EU Project INSYSME, 2016; Ahmadi, Dusi and J. Gough., 2017; Petrović, Stojadinović and Mojsilović, 2017; Verlato, 2017; Mojsilović, Petrović and Stojadinović, 2019). These layers can be horizontal, inserted between the bricks or between the panel and the beam of a frame, or vertical, placed between the infill panel and the columns (Figure 1).

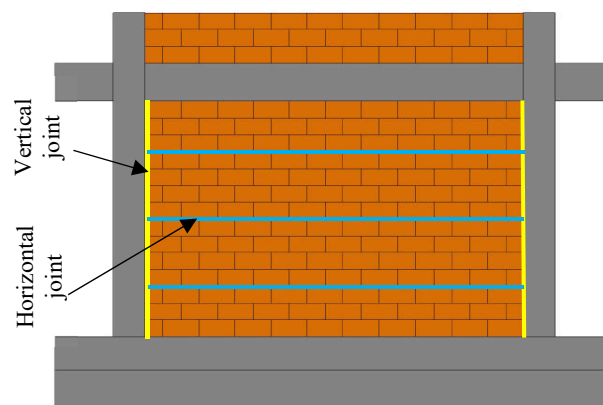


Figure 1. Masonry infilled walls with horizontal and vertical joints.

Among the different materials that can be employed for the soft layers, rubber is one of the most promising, because of the wide range of stiffness and dissipation capacity achievable by the choice of suitable compound and geometry. The Tun Abdul Razak Research Centre (TARRC) has developed an innovative layer (Figure 2) with a high-damping rubber compound. The rubber layer does not require skilled labour to be deployed (Figure 3a) and its effectiveness was proved during tests carried within the European research project INSYSME (EU Project INSYSME, 2016) (INnovative SYStems for earthquake-resistant Masonry Enclosures in reinforced concrete buildings) on seismic protection of infill walls (Figure 3b).



Figure 2. Rubber joints developed by TARRC (Ahmadi, Dusi and J. Gough., 2017)



(a)

(b)

Figure 3. (a) Demonstration of TARRC's rubber wall joint deployment at SAIE Bologna (SAIE, 2015) (b) Masonry infilled frame with horizontal and vertical rubber joints tested within INSYSME project (EU Project INSYSME, 2016)

However, the in-plane and out-of-plane quasi-static tests carried out at University of Padova during INSYSME project demonstrated only the “proof of concept” of the technology. Thus, in order to increase the technology readiness level of the device and promote its use in real practice, further experimental and numerical investigations are needed to fill some existing gaps of knowledge. These gaps concern mainly the dissipation capabilities of the joints and of systems equipped with them, and the strength of the bond between the rubber and the mortar. For this reason, an extensive experimental campaign was carried out at the University of Strathclyde, thanks to the creation of an unconventional experimental setup that allowed evaluating the cyclic behaviour of masonry triplets with mortar and rubber joints.

The results of this investigation, described in this report, provide a better understanding of the mechanical properties of mortar-rubber joints. They are also useful to inform numerical studies aimed at characterising the dynamic behaviour of RC frames with masonry infill and rubber joints. On this regard, in the last decades, significant research effort has been directed towards the development of finite element (FE) models for the analysis of traditional masonry components. These include macro models (Pietruszczak and Niu, 1992; El-Dakhkhni, Drysdale and Khattab, 2006; Calìò, Marletta and Pantò, 2012; Uva *et al.*, 2012; Calìò and Pantò, 2014; Pantò, Calìò and Lourenço, 2017; Nicoletti *et al.*, 2020; Ruggieri, Porco and Uva, 2020; Ruggieri *et al.*, 2021), micro models (Pantò, Calìò and Lourenço, 2017), discrete-element models (Sarhosis, Tsavdaridis and Giannopoulos, 2014), and meso-scale models (Lourenço, 1997; Lourenço and Rots, 1997; Dolatshahi and Aref, 2011; Macorini and Izzuddin, 2011, 2013, 2014; Nasiri and Liu, 2017). Some finite element studies have been carried out to evaluate the behaviour of masonry infill walls with soft or sliding joints (Preti, Bettini and Plizzari, 2012; Mojsilović, Petrović and Anglada, 2015; Vögeli, Mojsilović and Stojadinović, 2015; Petrović, Stojadinović and Mojsilović, 2017; Di Trapani *et al.*, 2020), but the case of rubber joints has not been fully investigated yet. A preliminary study by some of the authors of this report (Dhir *et al.*, 2021) has focused on the quasi-static behaviour of RC frames with masonry infills. The results of the experimental campaign can be used to further expand this modelling strategy in order to investigate how the damping capabilities of the joints can be effectively used to reduce the seismic demand imposed on RC infilled frames.

The rest of the report is organized as follows. Section 2 describes the various tests carried out to characterize the behaviour of the single components of the masonry triplets (bricks, mortar, and rubber layers), and of the masonry triplets. Section 3 describes the numerical simulations of these tests, carried out in Abaqus (Systèmes, 2016) using a micro-modelling approach. Section 4 summarises previous work carried out by the authors of this report in the field of advanced and simplified modelling of RC frames with masonry infill wall and rubber joints and discusses how the results of the experimental campaign of Section 2 can be used to inform these modelling strategies. The report ends with a Conclusions and future works section.

2. EXPERIMENTAL CAMPAIGN

Unreinforced masonry is a composite of blocks/bricks with mortar joints, whose overall behaviour is influenced by several factors, such as: brick and mortar properties, brick size and aspect ratio, joint thickness, joint orientation, relative position of head and bed joints, properties of the unit/mortar bond and workmanship (joint quality) (Sutcliffe, Yu and Page, 1999). Failure of masonry structures may occur in the bricks, in the mortar or at their interface. Cracking and crushing may occur in the brick and/or in the mortar. Two main failure modes are possible for the brick/mortar interface, namely tensile failure and shear failure, or by a combination of these. Tensile failure leads to joint opening and shear failure to joint sliding with friction. In the case of mortar-rubber joints, the rubber properties and the bond between the rubber and the mortar play also an important role in the overall behaviour of the composite system. Failure may occur in correspondence of the various components or at the interfaces between these components. Thus, in order to fully characterize the behaviour and capacity of masonry triplets, it is necessary to understand the behaviour of the single components as well as the bond properties.

Section 2.1 and Section 2.2 describe the characterization tests for respectively bricks and mortar, and for the rubber compound. Finally, Section 2.3 describes the apparatus developed for testing the triplets, and Section 2.4 the tests on the triplets with mortar joints and with mortar-rubber joints.

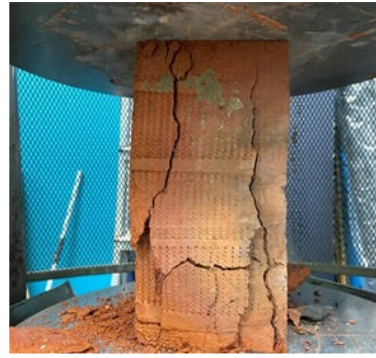
2.1. Brick and mortar characterization

In this study, standard fired bricks (Birtley Old English Bricks) with dimensions of 215 x 102.5 x 65 mm³ were used. Although these bricks are only one of the many types of bricks and blocks employed in masonry infill wall construction, they were chosen because they were easy to get locally, and because the main aim of the study was to investigate the behaviour of the joints, and thus the type of brick employed was not too important.

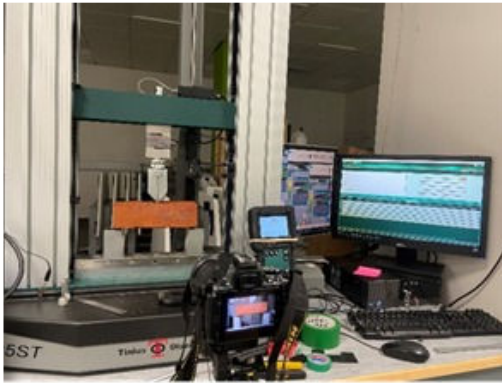
The fired clay bricks were tested under uniaxial compressive loading along the horizontal and vertical directions (Figure. 4a, b). A three-point bending test was also carried out on the brick units to estimate the flexural strength (Figure. 4c-e) and the load displacement relation is presented in Figure. 4f. The test results are summarized in Table 1.



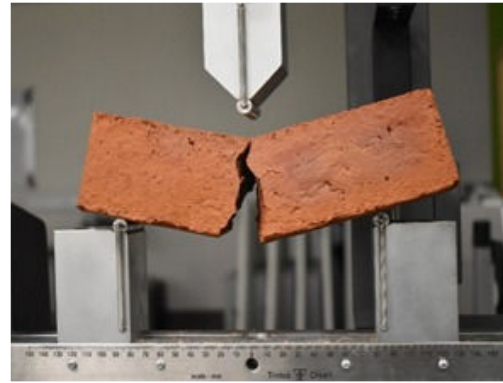
(a)



(b)



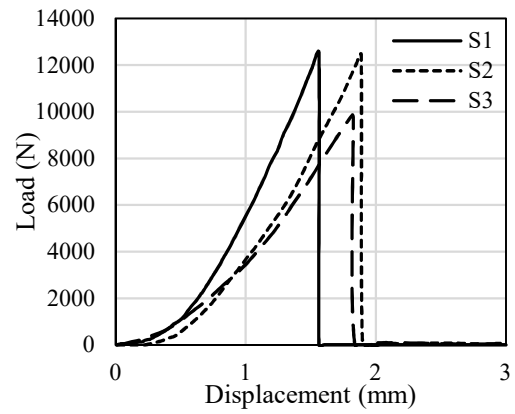
(c)



(d)



(e)



(f)

Figure. 4. (a, b) compressive strength test on bricks in horizontal and vertical direction (c) test setup for three-point bending test of brick specimens (d, e) failed brick specimens (f) load-displacement response of brick specimens

Table 1. Mechanical properties of clay brick specimens

Three-point bending test				Compressive strength					
				Horizontal direction			Vertical direction		
Samples	Density (Kg/m ³)	R_f [N]	f_f (MPa)	Samples	f_c (MPa)	E_b (MPa)	Samples	f_c (MPa)	E_b (MPa)
S1	2043	12523	9.38	BH_1	16.2	20125	BV_1	11.4	16882
S2	2094	12440	12.03	BH_2	15.2	19493	BV_2	12.6	17748
S3	2078	9774	11.27	BH_3	14.7	19170	BV_3	11.1	16658
Avg.	2072	11579	10.91		15.37	19596		11.7	17096

The same general-purpose ready-mix mortar (Cement: Sand = 20-25%: 75-80%) was used for the various triplets. The mortar was prepared with a water to cement ratio of 0.8:1 to ensure cement hydration and lubrication of sand particles. In order to characterise the mechanical behaviour of mortar, both flexural strength tests (Figure 5) and cube compressive strength tests (Figure 6) were conducted. Mortar specimens were left to cure at a temperature of about 25⁰C for 28 days.

For the flexural strength tests of mortar, a total of 6 mortar beams of size 40 x 40 x 160 mm³ were considered. These beams were subjected to three-point bending tests at a constant displacement rate of 0.05 mm/min (Barattucci *et al.*, 2020). The flexural strength f_f of all mortar samples was calculated following EN (EN 1015-11, 2006) as follows:

$$f_f = \frac{3 R_f l}{2 b h^2} \quad (1)$$

where R_f is the peak load, l is the span length, b and h are the width and height of the vertical cross-section of the mortar sample, respectively.

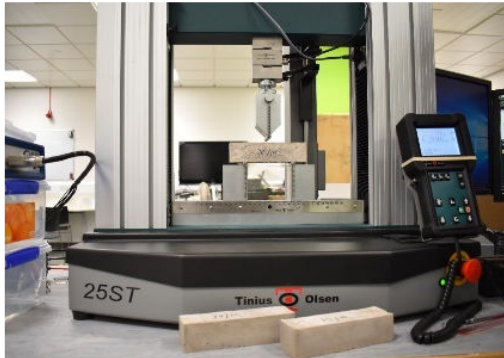
Similarly, a total of 6 mortar cubes of size 50 x 50 x 50 mm³ were cast and subjected to compressive strength tests. The mortar cubes were tested on the 28th day since casting at a constant displacement rate of 0.10 mm/min (Barattucci *et al.*, 2020). Figure 7a and Figure 7b show the three-point bending and compressive peak strengths occurred at increasingly higher strains. Table 2 summarises the values of the mortar mechanical properties from the various tests as well as the average ones.



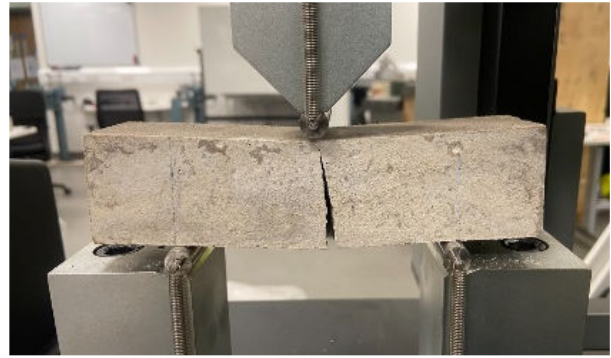
(a)



(b)



(c)



(d)



(e)



(f)

Figure 5. (a, b) Casting (c, d) testing (e, f) failed mortar specimens for the three-point bending test (at 28 days)

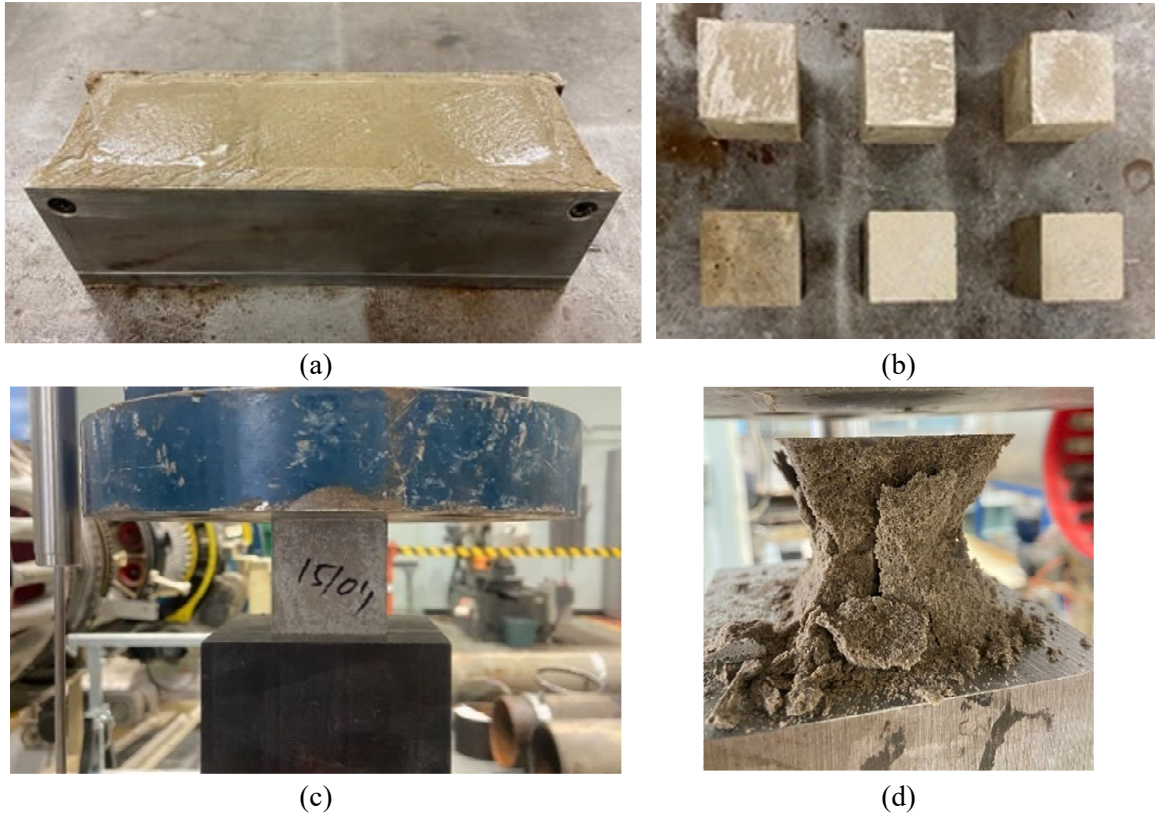


Figure 6. (a, b) Casting and preparation (c, d) testing of mortar cubes for 28-days Compressive strength tests

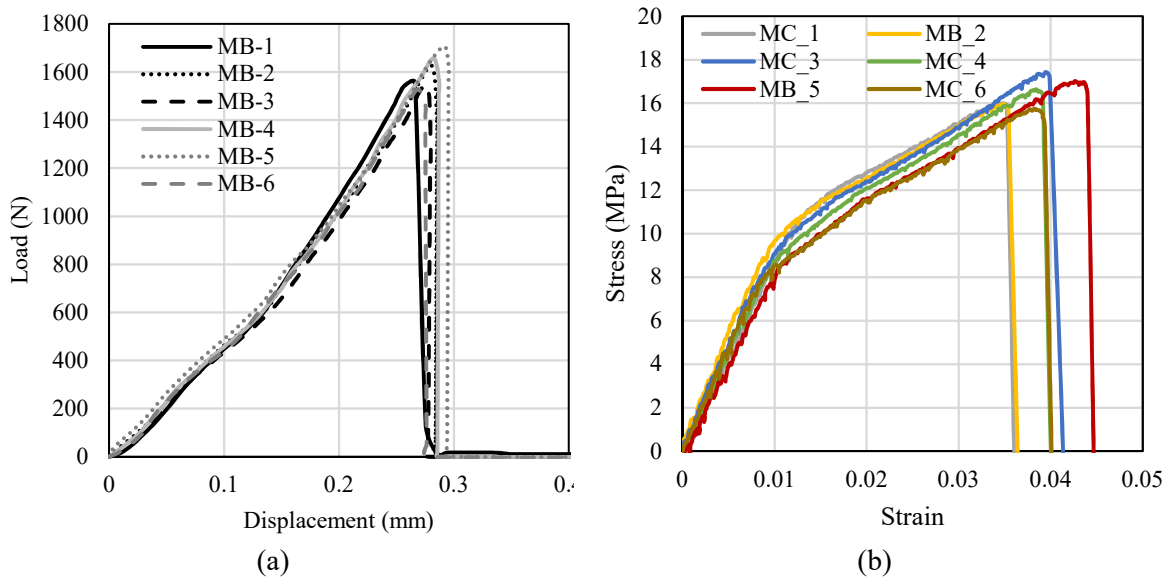


Figure 7. (a) Three-point bending of mortar beams (b) compression tests of mortar cubes at 28 days.

Table 2. Mechanical properties of mortar specimens

Three-point bending test				Compressive strength		
Samples	Density (Kg/m ³)	R_f [N]	f_t (MPa)	Samples	f_c (MPa)	E_m (MPa)
MB_1	2043	1556.18	3.65	MC_1	16.01	1780.87
MB_2	2094	1622.60	3.80	MC_2	15.95	1629.09
MB_3	2078	1547.13	3.63	MC_3	17.43	1875.38
MB_4	2063	1657.50	3.88	MC_4	16.64	1780.00
MB_5	2086	1706.73	4.00	MC_5	17.05	1832.10
MB_6	2070	1528.25	3.58	MC_6	15.74	1709.00
Avg.	2072	1603.06	3.76	Avg.	16.47	1767.74

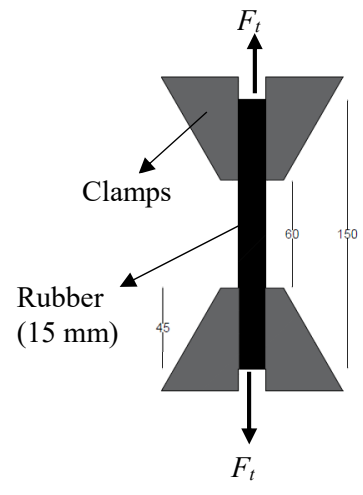
2.2. Characterisation of rubber joints

The horizontal deformable joints are the core element of the proposed system. During the experimental campaign, DRES-V2 joints (Verlato, 2017) (Figure 2) were used. These joints have thickness 15 mm, width 300 mm, and height 500 mm. Even if sliding can be considered an excellent mechanism to both reduce infill damage and increase energy dissipation (Morandi, Milanesi and Magenes, 2016), at the same time it does not tend to “auto-recover”, without specific devices, residual displacements. To improve this aspect, small pins (see Figure 2) were distributed on the surface of the rubber joints in order to enhance the bond with the mortar and prevent unwanted joint sliding at low drift levels.

A tensile test was performed (Figure 8a) on a rubber specimen (150 mm length, 25 mm width and 15 mm thick) prepared from the rubber joint sheets (see Figure 2) in the testing machine (Tinius Olsen) where, Figure 8b shows the schematic diagram for the test setup. Figure 8c and Figure 8d shows the deformed shape of the rubber specimen during and after the completion of the test. The hysteretic response of the specimen during the loading and un-loading cycle with the introduction of very low delay is presented in Figure 8e. Figure 8f shows the results of the relaxation test, which was performed by pulling the specimen up to 100% of its length and holding it in this position for 24 hours while measuring the change of resisting force. This is because after the initial seconds of hold time, when a very rapid decrease in stress is observed, the stress decreases at a very slow pace and it can take a long time before a constant asymptotic value is reached.



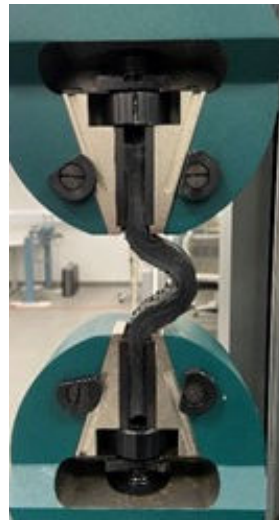
(a)



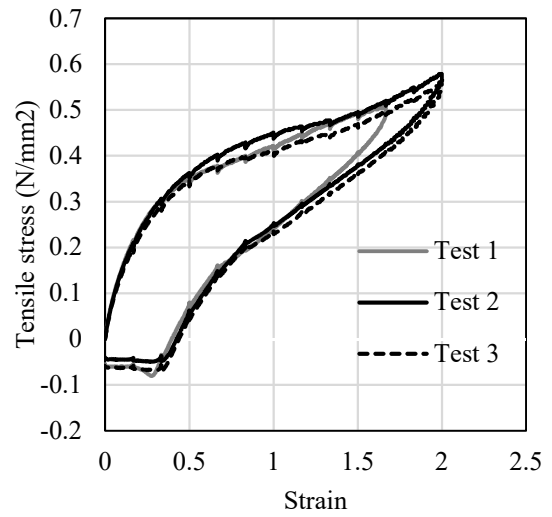
(b)



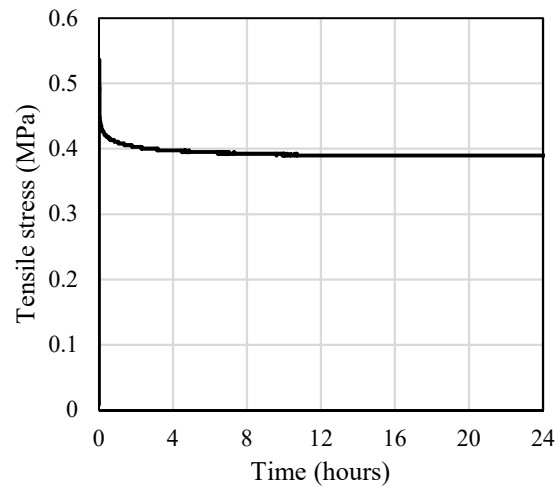
(c)



(d)



(e)



(f)

Figure 8. (a, b) tensile test setup of rubber specimen (c, d) deformed shape before and after the test (e) tensile stress- strain response (f) relaxation test.

In order to study the behaviour of the rubber compound under simple shear, a quadruple specimen was prepared (see Figure 9a). Figure 9b shows the testing of the rubber quadruplet and Figure 9c the deformed shape during the test. Figure 10a illustrates the shear stress-strain response of the quadruple specimen at different amplitudes of load cycles. The relaxation test on the rubber quadruplet is presented in Figure 10b.

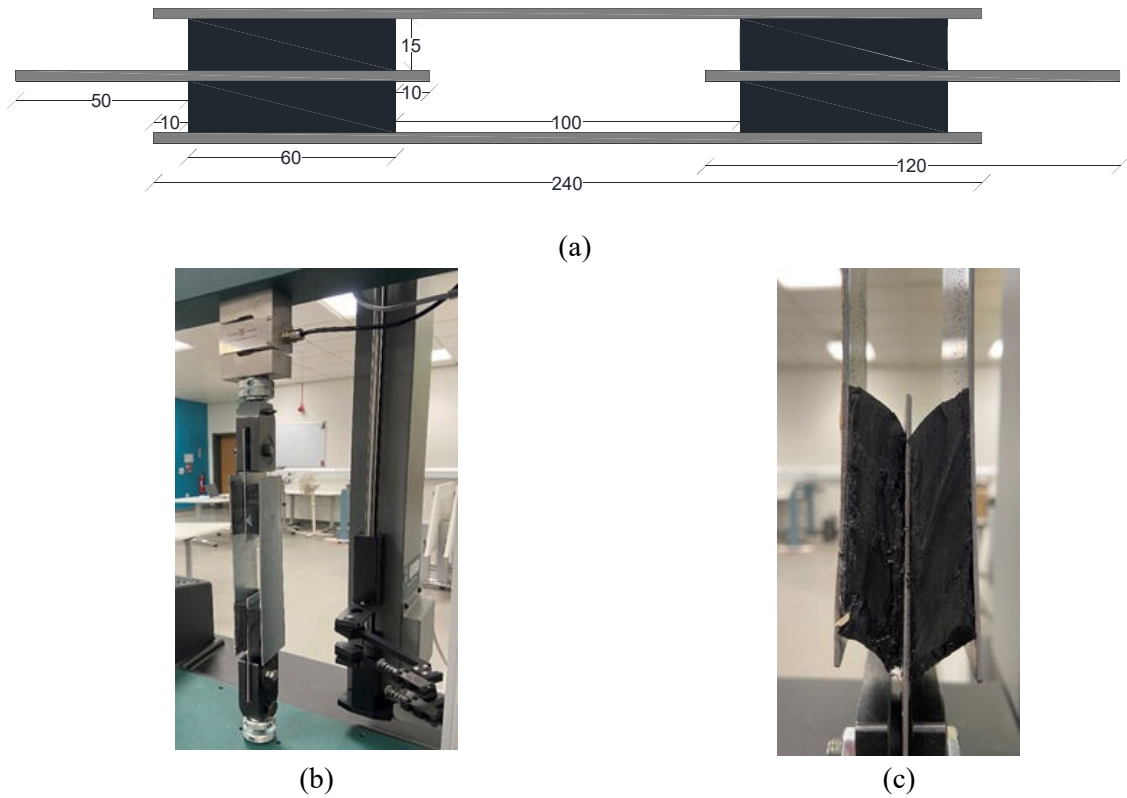


Figure 9. (a) detailed dimension (b) test setup (c) deformed shape of the quadruplet

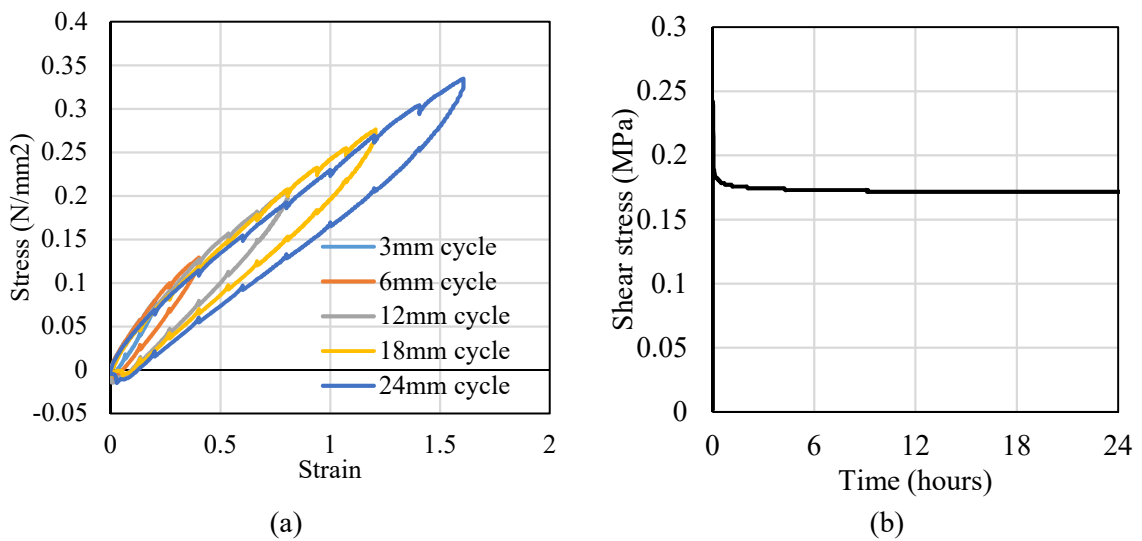


Figure 10. (a) Shear stress-strain response (b) relaxation test on rubber quadruplet

2.3. Manufacturing of masonry triplets and experimental tests set-up

Masonry triplets were manufactured by bonding standard fired clay bricks (Birtley Old English Bricks) of dimensions of 215 x 102.5 x 65 mm³ (see Figure 11a, Figure 11b) with the ready-mix cement mortar (20-25% cement: 70-75% sand) prepared with water to cement ratios of 0.8 to ensure suitable workability and a good mechanical performance (Singh, Munjal and Thammishetti, 2015). A total of 42 masonry triplets were prepared among which with 12 samples were with mortar joints and 30 with mortar-rubber joints.

Masonry triplets with mortar joints were manufactured with three bricks bonded together by two 10 mm-thick mortar joints, as shown in Figure 11e, leading to masonry triplets with dimensions of 215 x 215 x 102.5 mm³ (Figure 11c). Similarly, triplets were prepared with dimensions of 215 x 265 x 102.5 mm³ (Figure 11d) for mortar-rubber joints, with the rubber layers sandwiched between two layers of 10 mm thick mortar, as shown in Figure 11f. Prior to manufacturing, all bricks were submerged in water for a minimum time of 24 h to ensure an optimised bonding with the mortar joints and to avoid quick drying of the samples with a consequent formation of cracks. Bricks were then wiped with a dry cloth before proceeding with the laying of the mortar joints. Special care was taken to build the masonry triplets as straight as possible to avoid spurious eccentricities that could affect the shearing tests. After manufacturing, masonry triplets were left to cure for a minimum time of 28 days in laboratory at a temperature of about 25°C. After curing, the masonry triplets were subjected to shear mechanical tests at different compression levels.



(a)



(b)

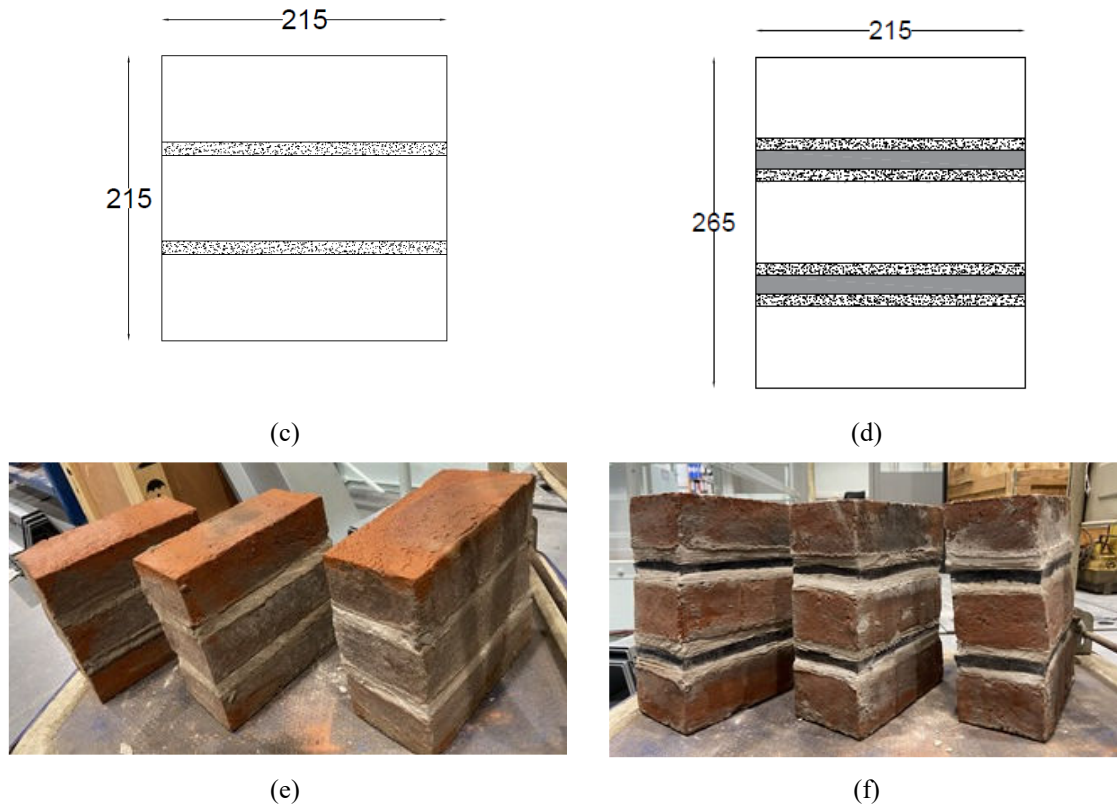
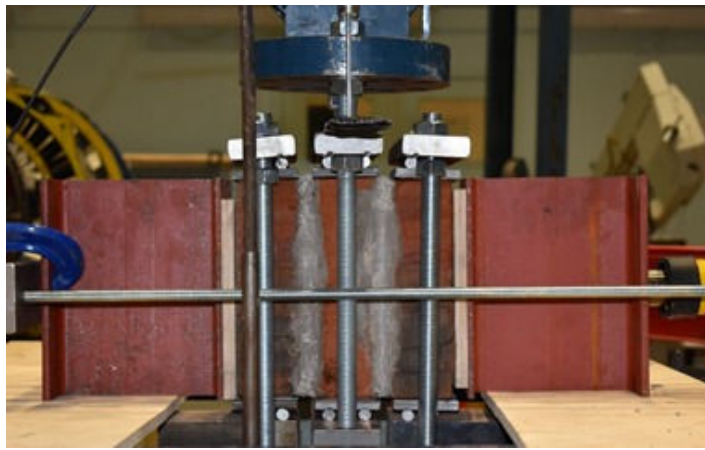


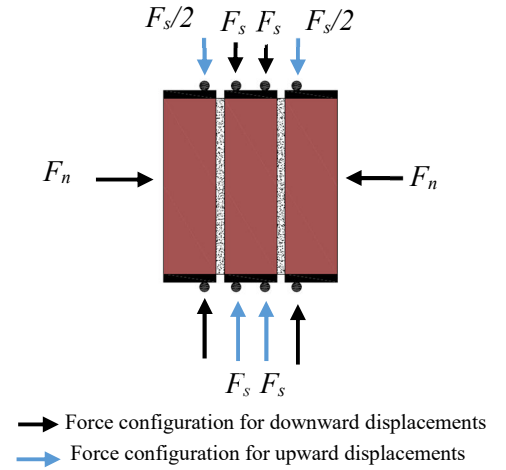
Figure 11. (a) Typical Birtley old English bricks used (b) rubber joints (c, d) dimensions of the triplets with mortar and mortar-rubber joints (e) triplet with mortar joint (f) triplets with mortar-rubber joints

In order to characterize the cyclic behaviour of the triplets, the basic shear test set-up proposed by the European Standard EN (EN 1052-3, 2002) was modified and expanded as shown in Figure 12a. The novelty of the proposed testing apparatus consists in the possibility of applying shear loadings in both downward and upward directions (Figure 12b) and not only in the downward one.

Figure 13 describes the assembly of the testing apparatus and the various components. A hydraulic jack is used to apply the horizontal compressive stress on the masonry triplets. The compressive stress is applied before the shearing displacement, and it is kept constant during the entire duration of the test. The shearing vertical displacement is applied through a computer-controlled actuator (Figure 12a) with a maximum load capacity of 250 kN. The testing programme consisted of performing monotonic and cyclic shearing on three triplets for each levels of confinement (0.2, 0.4 and 0.6 MPa), for a total of nine masonry triplets with mortar joints and nine triplets with mortar-rubber joints tested.



(a)



(b)

Figure 12. (a) Shear test set-up (b) forces configuration for cyclic shear test

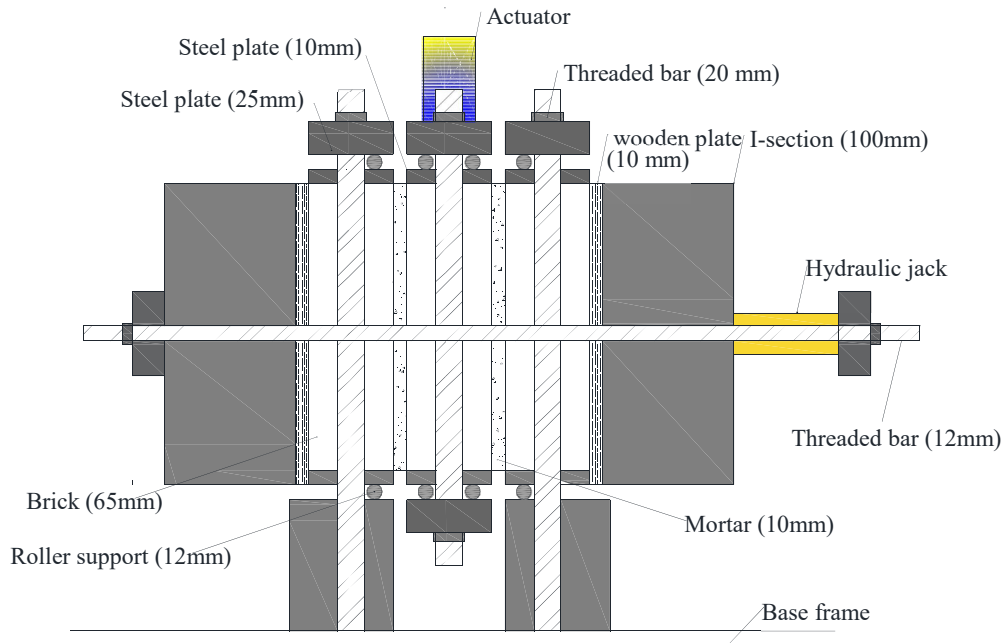


Figure 13. Testing equipment apparatus used to perform shearing tests on triplet specimens.

2.4. Monotonic and cyclic shear tests of triplets

The monotonic test was carried out by imposing a constant downward displacement rate of 1 mm/min through the actuator. The cyclic test was carried out by alternatively imposing downward and upward displacements on the intermediate brick over five cycles. Figure 14 shows the load-displacement relationship of the triplets with mortar joints under monotonic and cyclic shear. It can be seen that the initial stiffness of the system is not affected by the pre-compression level, while the peak load increases for increasing pre-compression level.

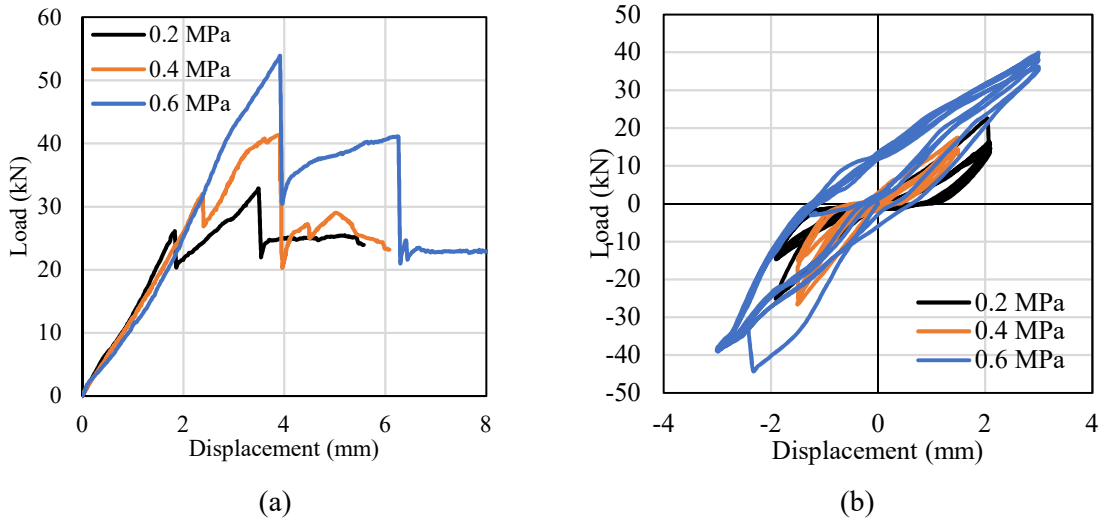


Figure 14. (a) Monotonic (b) Cyclic shear response of triplets with mortar joints

Figure 15, Figure 16 and Figure 17 show the failed specimens at the end of the monotonic and cyclic tests carried out at different levels of pre-compression. It can be seen from these results that the failure occurred at the mortar-brick joint interface, which was found to be weaker than the mortar layers and the bricks.

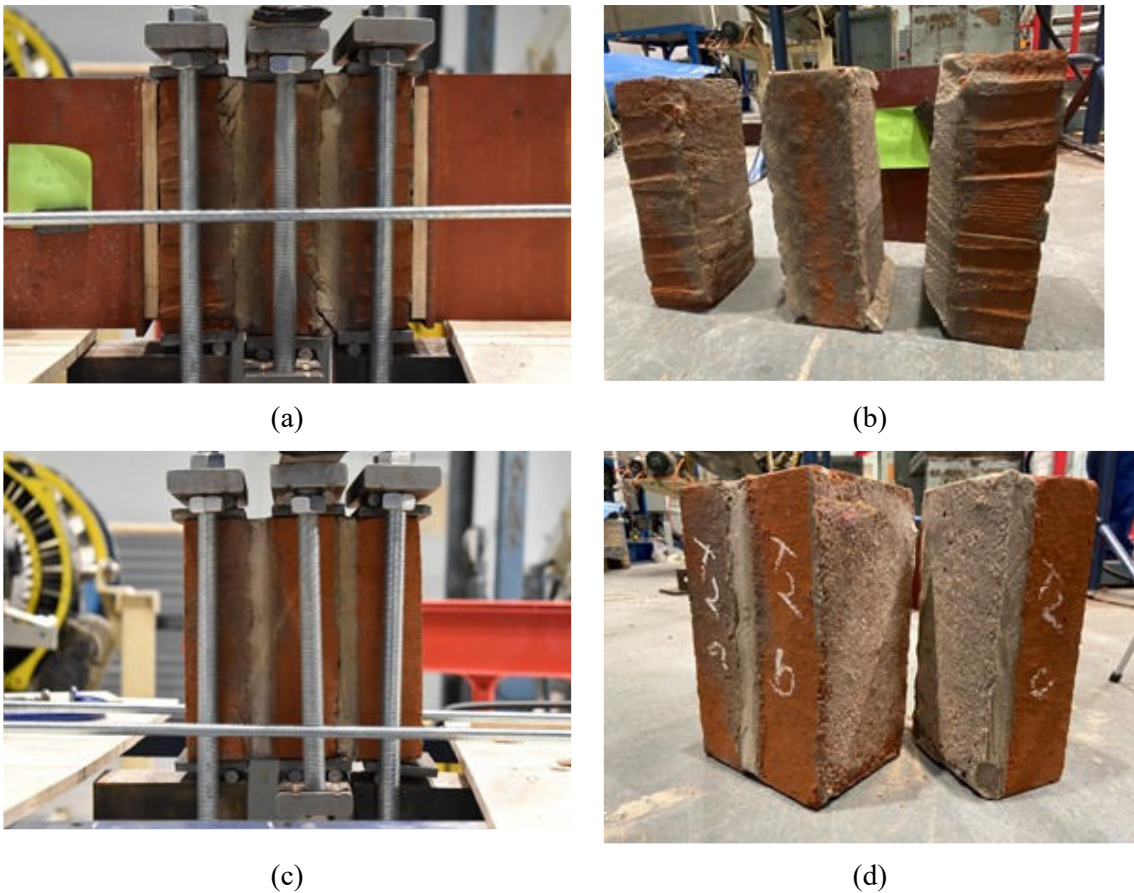


Figure 15. (a, b) Monotonic (c, d) Cyclic shear test of mortar triplets with 0.2 MPa pre-compression



(a)



(b)



(c)



(d)

Figure 16. (a, b) Monotonic (c, d) Cyclic shear test of mortar triplets with 0.4 MPa pre-compression.



(a)



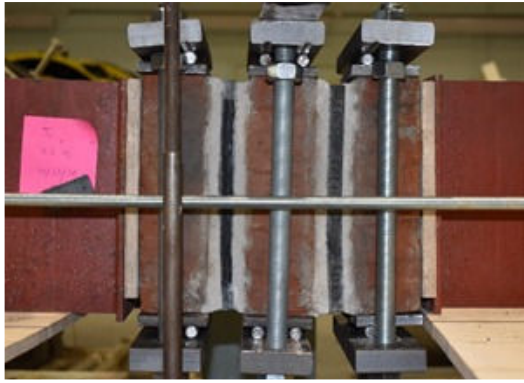
(b)



Figure 17. (a, b) Monotonic (c, d) Cyclic shear test of mortar triplets with 0.6 MPa pre-compression

The triplets with rubber-mortar joints were tested under both monotonic and cyclic shear loading. Figure 18 shows the cyclic shear test setup and test specimens. Figure 19a shows the load-displacement of the triplets with mortar-rubber joints under monotonic shear. Compared to the triplets with mortar joints (Figure 14a), the triplets with mortar-rubber joints exhibit significantly lower stiffness, lower peak load capacity (about one fifth), and a less brittle post-peak response. This is an important and useful feature of the mechanical behaviour of mortar-rubber joints, since it allows to increase the flexibility of masonry infills and to reduce the interaction between the infill and the frame while reducing the forces induced by the earthquake in the system for a given drift demand. Figure 19b-d show the cyclic shear response of the triplets with mortar-rubber joints obtained for different levels of pre-compression and different amplitudes (10 mm, 15 mm and 20 mm). It can be observed that the stiffness of the system increases slightly for increasing levels of precompression, whereas the dissipated energy does not change significantly.

In order to better describe the effects of the precompression level and amplitude of oscillation on the hysteretic behaviour of the system, Figure 20 shows the variation of the secant shear modulus and equivalent damping ratio for increasing apparent shear strains (i.e., the shear displacement divided by the rubber layer height) and for different precompression levels. As already observed, these two quantities are not significantly affected by the precompression level, whereas they are strongly influenced by the amplitude of shear deflection. In fact, the secant stiffness reduces significantly with the amplitude of shear strain, whereas the damping ratio increases. Overall, the rubber joints exhibit very good dissipative properties, with high damping ratio values thanks to the use of a high-damping rubber compound.

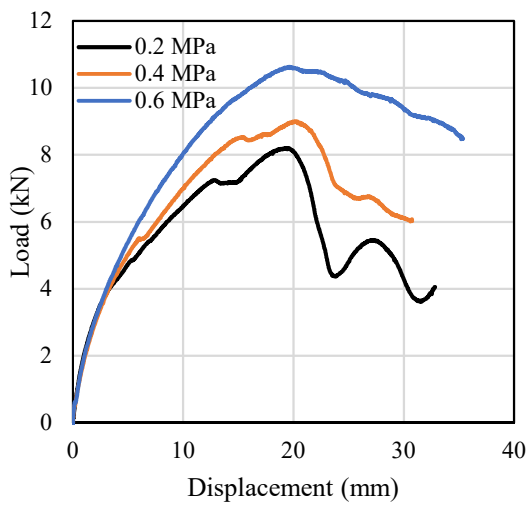


(a)

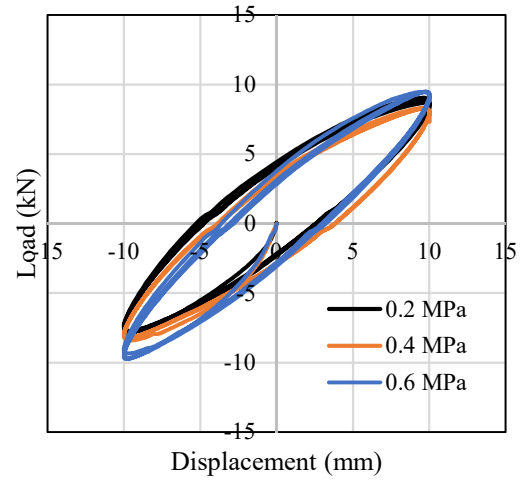


(b)

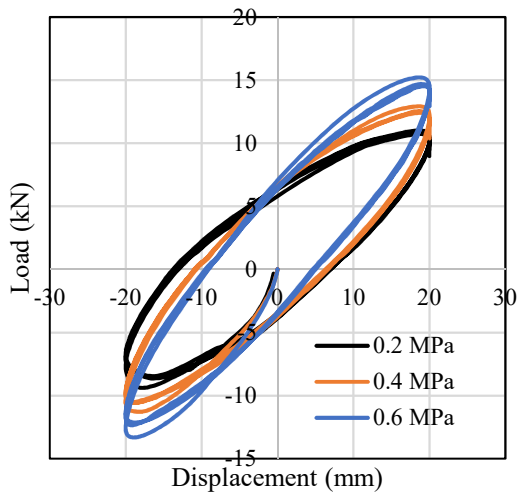
Figure 18. (a) Cyclic shear test setup (b) test specimens.



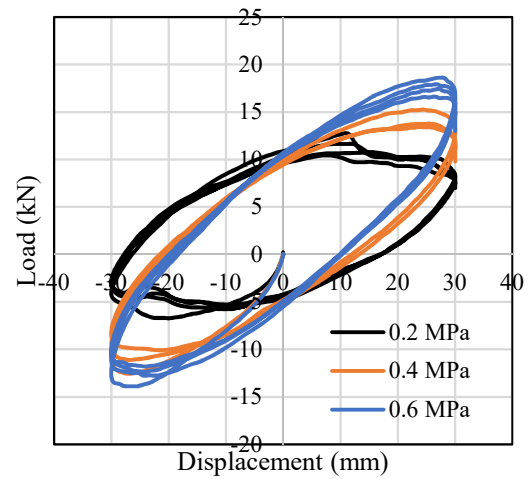
(a)



(b)



(c)



(d)

Figure 19. Shear response of triplets with mortar-rubber joints for various levels of pre-compressions: monotonic loading (a) and cyclic loading (b, c, d)

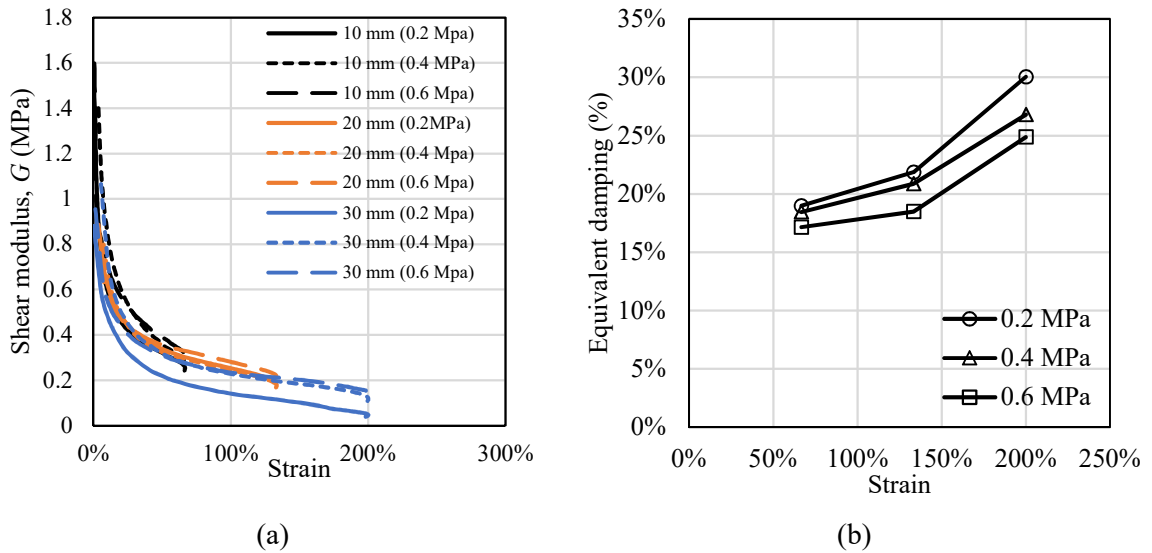
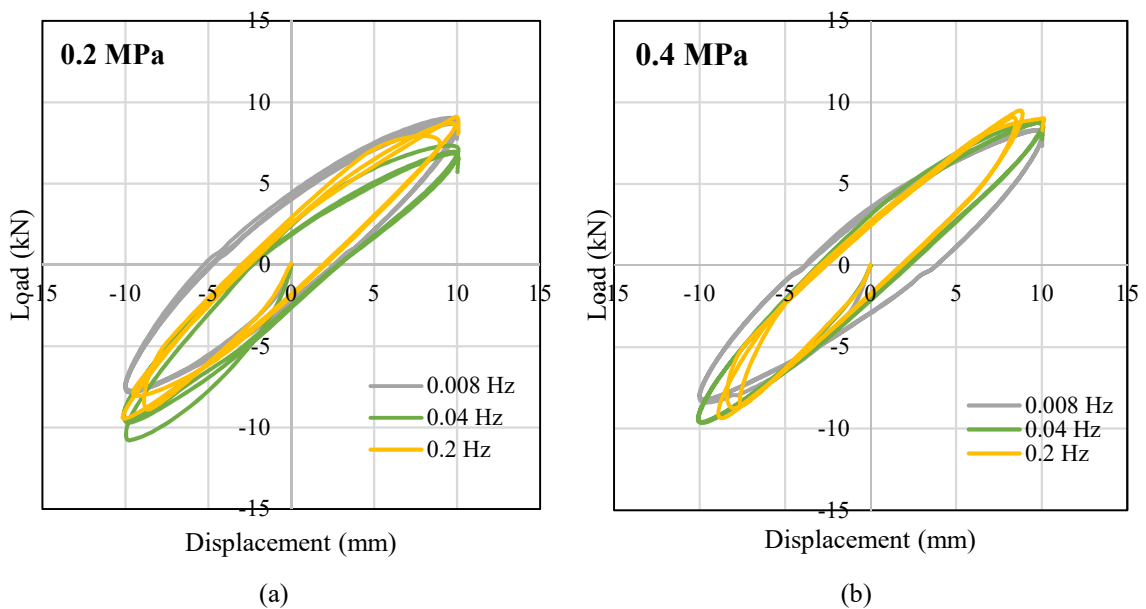
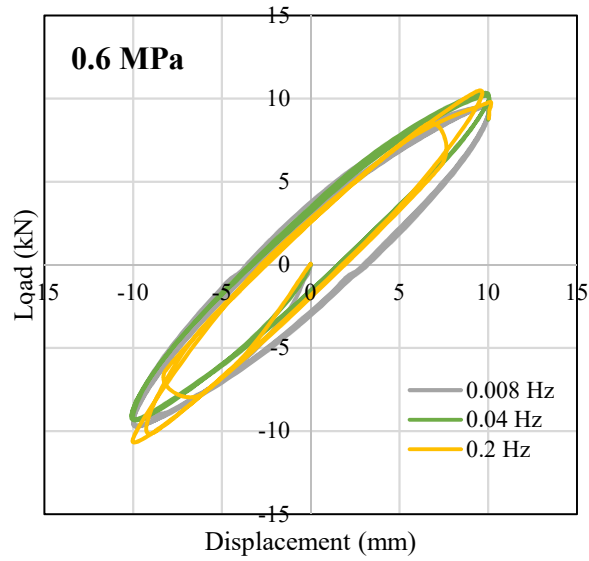


Figure 20. Variation of the (a) secant shear modulus (b) equivalent damping with increasing shear strain at different compression levels.

Figure 21 shows the cyclic shear response obtained for different frequencies of oscillation. It can be seen from Figure 21 that the stiffness of the mortar-rubber joint and the energy dissipation capacity are not significantly affected by the frequency. It is noteworthy that it was not possible to test higher frequencies, that may be more representative of those characteristics of earthquake response of RC buildings with infills (i.e. higher than 1Hz).

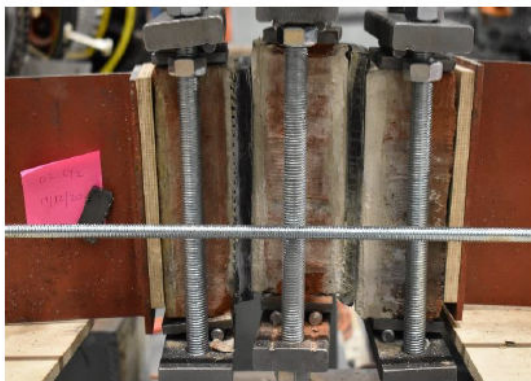




(c)

Figure 21. Cyclic shear response of triplets with mortar-rubber joints tested under various frequencies of oscillation for different precompression levels: (a) 0.2 Mpa (b) 0.4 MPa and (c) 0.6 MPa.

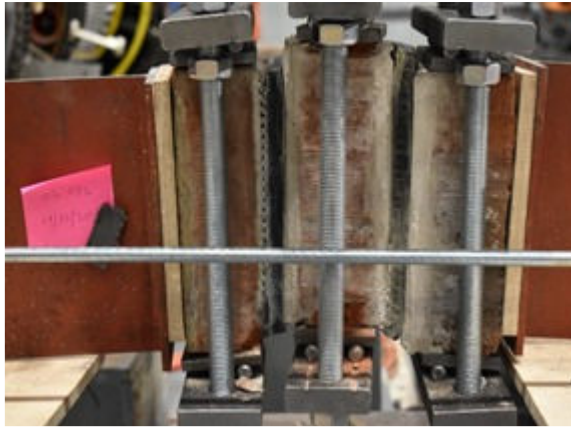
Figure 22, Figure. 23 and Figure 24 show the various failed specimens at the end of the tests. It can be seen that failure occurred at the rubber-mortar interface, which was found to be the weakest component in the system.



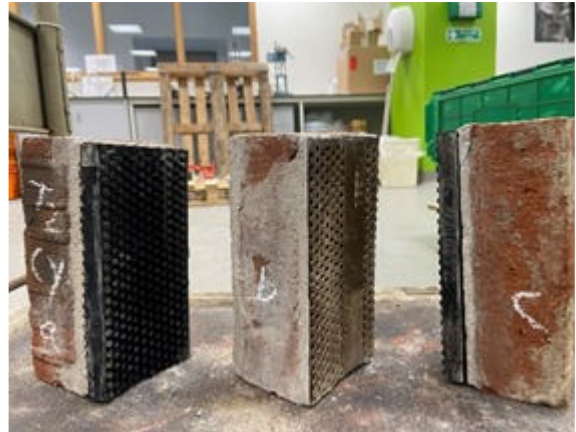
(a)



(b)



(c)



(d)

Figure 22. (a, b) Monotonic (c, d) Cyclic shear test of innovative triplets with 0.2 MPa pre-compression



(a)



(b)



(c)



(d)

Figure 23. (a, b) Monotonic (c, d) Cyclic shear test of innovative triplets with 0.4 MPa pre-compression

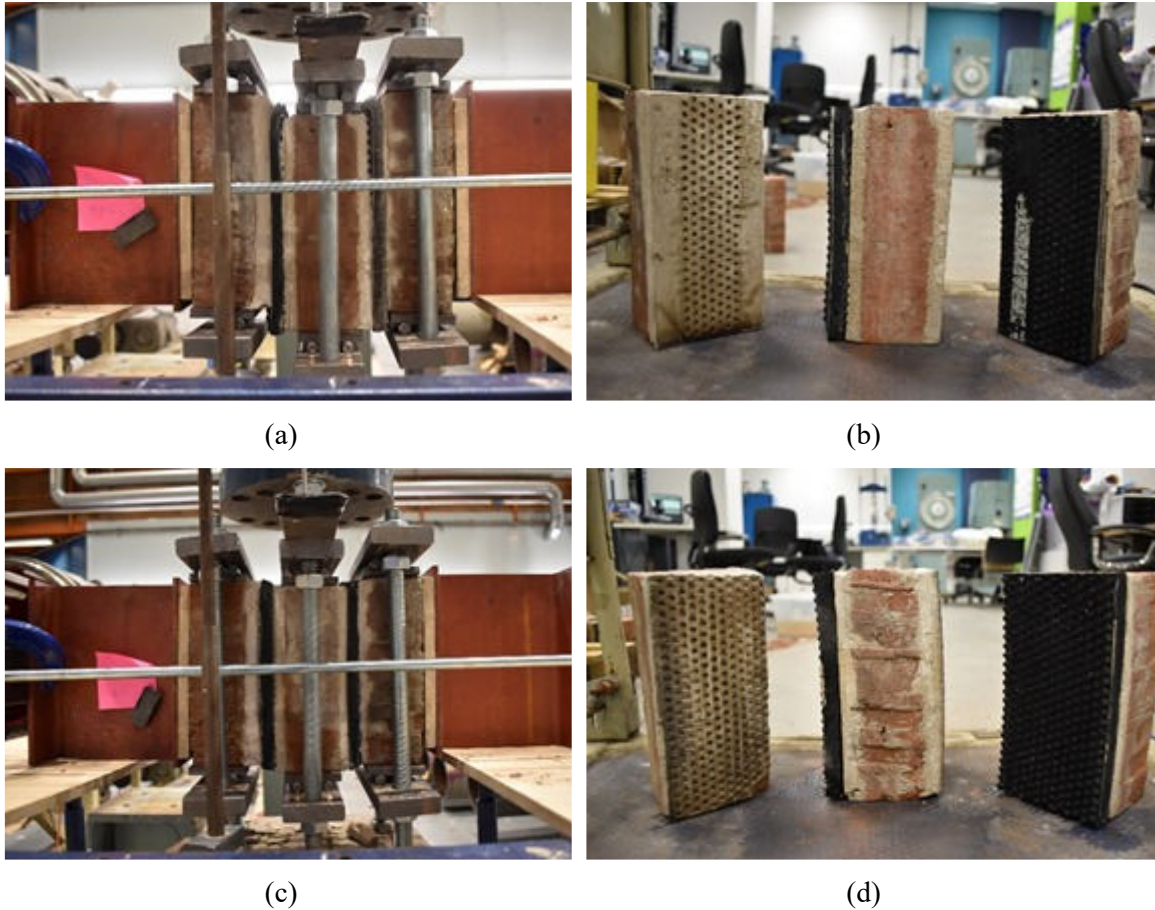


Figure 24. (a, b) Monotonic (c, d) Cyclic shear test of innovative triplets with 0.6 MPa pre-compression

Table 3 reports the both peak loads of the masonry triplets exhibited in the monotonic tests, for different levels of pre-compression. Figure 25 shows the relationship between the peak shear strengths, calculated as the ratio between the peak shear strength and two times the cross-sectional area of the interface, and the pre-compression stress, for the two types of masonry triplets. The experimental data can be interpolated with straight lines that represent the well-known Mohr-Coulomb failure criterion, expressed as:

$$\tau = c + \sigma_p \tan(\phi) \quad (2)$$

where σ_p is the shear strength, c is the cohesion, and ϕ is the friction angle. Table 3 shows the values of cohesion and friction angle providing the best fit of Eq.2 to the experimental data. It can be seen that these values of the parameters provide a very good fit to the test results. In general, the capacity of the mortar joint is 4-5 times higher than that of the mortar-rubber joint, due to the relatively weak bond between the rubber and the mortar.

Table 3. Peak load of masonry triplets subjected to monotonic shear tests.

Samples	Pre-compression (MPa)	Peak stress (MPa)	
		Mortar joints	Mortar-rubber joints
1	0.2	0.83	0.18
2	0.4	0.94	0.21
3	0.6	1.22	0.24

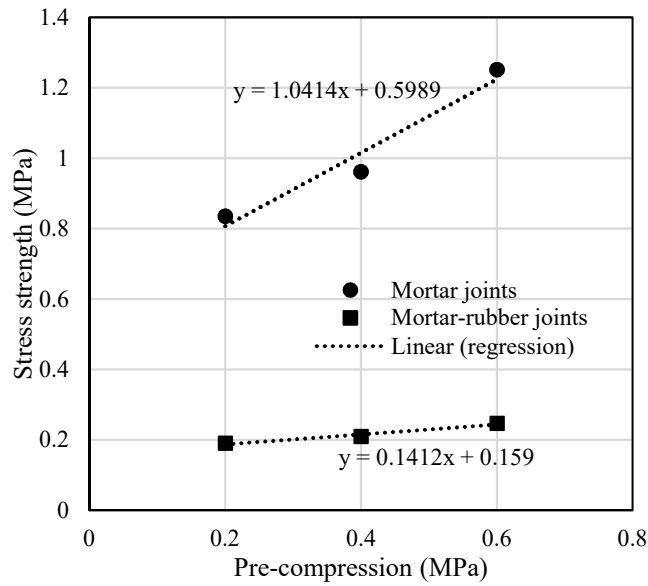


Figure 25. Relationship between shear strength and pre-compression stress for triplets

3. SIMULATION OF EXPERIMENTAL TESTS

This section illustrates the simulation of the experimental tests described in Section 2 carried out in the commercial FE software Abaqus (Systèmes, 2016) using a micro-modelling approach (Rots, 1997).

3.1 Simulation of experimental tests on triplets with mortar joints

The two components of the triplets (bricks and mortar layers) are described as a continuum, and discretised using 3D 8-noded solid elements (C3D8R). The behaviour of the mortar and the brick units is described using a Concrete Damage Plasticity (CDP) model (Lee and Fenves, 1998; *Concrete damaged plasticity*, 2017). Surface-to-surface contact interfaces are used to simulate the bond between the mortar layers. The cohesive interfaces exhibit initially a linear elastic response, followed by a cracking behaviour that describes the most critical failure modes, namely, tensile cracking and shear sliding. This allows simulating the failure occurred in correspondence of the brick-mortar interfaces for the mortar triplets. The parameters of the material and interface models

are based on the material characterisation tests and on the triplet tests discussed in the previous section. Table 4 and Table 5 illustrate the main parameters describing the mechanical properties of the brick units, the mortar layer, and the interfaces.

Table 4. Mechanical properties of the triplet components (brick and mortar units).

Mechanical properties	Brick units	Mortar
Young's modulus, E (MPa)	3000	1747
Poisson's ratio, ν (-)	0.1	0.15
Compressive strength, σ_c (MPa)	13.53	16.47
Strain at peak compressive stress	-	0.04
Peak tensile strength, σ_t (MPa)	1.57	1.74
Fracture energy in tension, G_f^I (MPa·mm)	0.07	0.09

Table 5. Properties of the contact interfaces describing the brick-mortar joints

Mortar Interaction Properties	Brick-mortar joints
k_n^m per unit area (N/mm ³)	1000
k_s^m, k_t^m per unit area (N/mm ³)	500
σ_t (MPa)	0.14
Cohesion, c (MPa)	0.6
Coefficient of friction, μ (-)	0.93
Normal fracture energy per unit area, G_f^I (MPa·mm)	0.015
Shear fracture energy per unit area, G_f^{II} (MPa·mm)	0.09

Figure 26 a shows the model developed for the triplets with mortar joints, using a fine mesh with element size of 10mm. Figure 26b shows the deformed shape of the model at failure and the plastic strain distribution, highlighting the high concentration of damage in correspondence of the mortar joints and the interface.

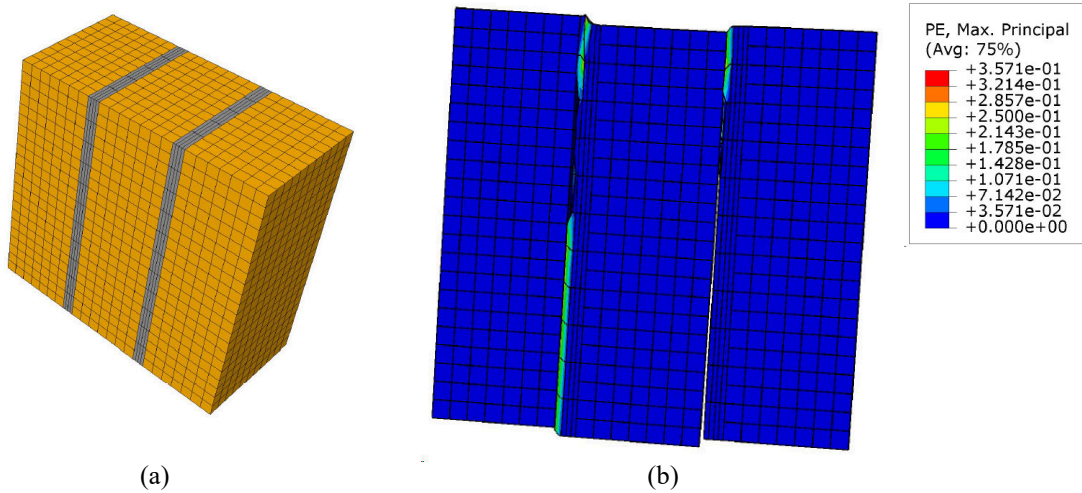
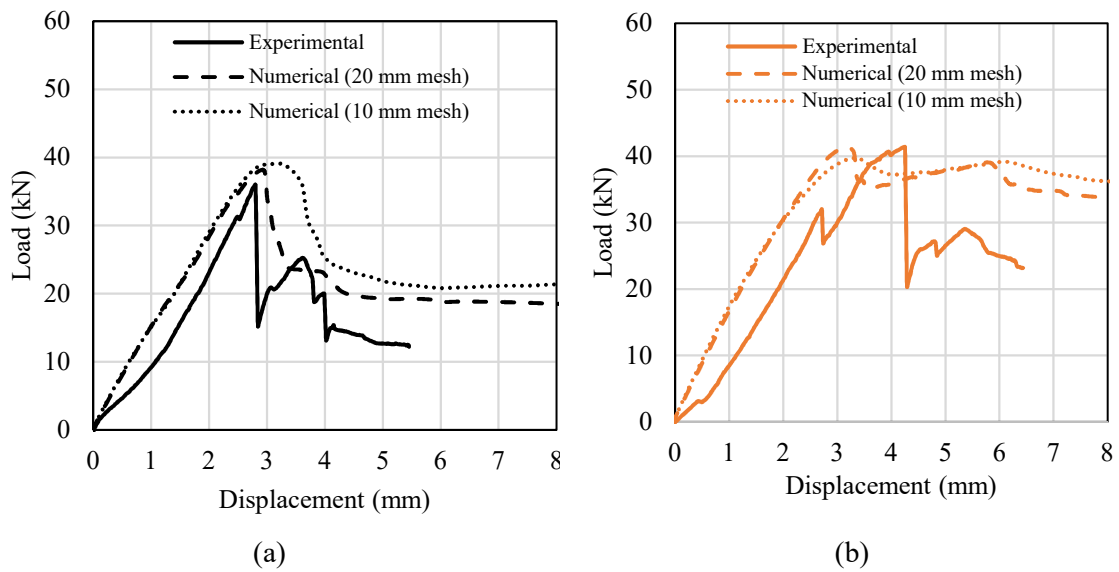


Figure 26. (a) FE model with refined mesh (b) plastic strain distributions for mortar triplets

Figure 27 compares the experimental and numerical responses of the masonry triplets with mortar joints under monotonic loading at different levels of pre-compression. Two different mesh sizes were considered (with characteristic element length of 10 mm and 20 mm) without noticing significant changes in the simulated response, which is quite well described by the proposed model.



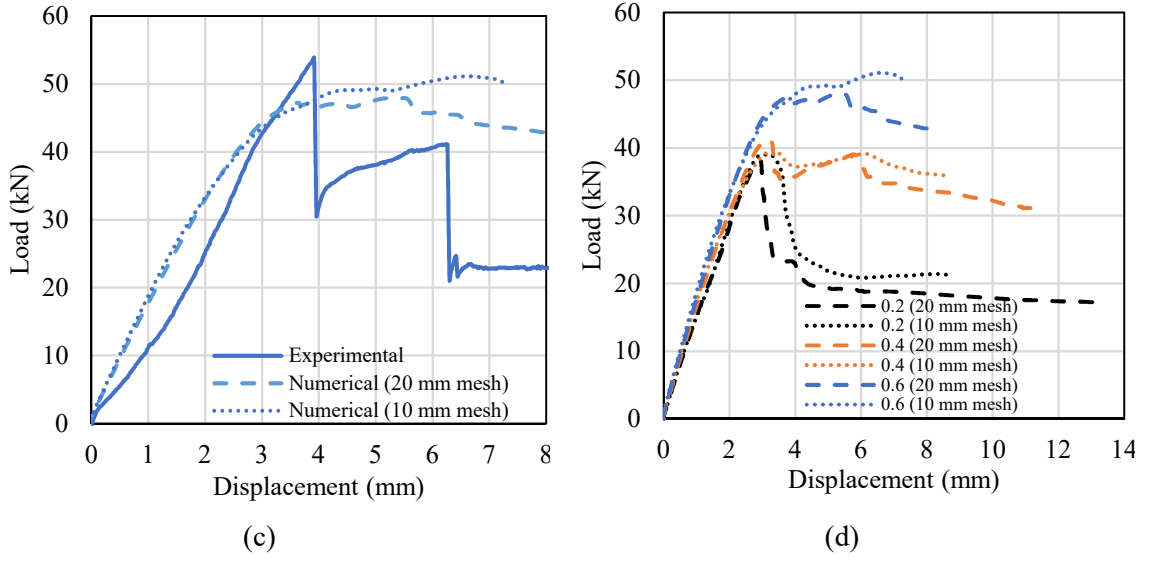


Figure 27. (a, b, c) Comparison of experimental and numerical response of the mortar triplets under monotonic loading at (a) 0.2 MPa (b) 0.4 MPa (c) 0.6 MPa pre-compression (d) Comparison of numerical responses only

3.2 Simulation of characterization rubber material tests and cyclic tests on triplets with mortar-rubber joints

This subsection describes the simulation and results of the uniaxial and double shear tests performed on rubber test pieces and the cyclic tests performed on triplets with mortar-rubber joint. The rubber is modelled using 3D 8-noded solid elements with a first-order hybrid formulation (C3D8H) to prevent volumetric locking, which is recommended to model the almost incompressible rubber material (Systèmes, 2016). Following the approach developed by Bergstrom and Boyce (Bergström and Boyce, 1998), the mechanical response of the rubber is described by two networks working in parallel. The first one, network A, corresponds to the time-independent behaviour of the rubber, which is described by a hyperelastic model. The other, network B, describes the non-linear rate-dependent part of the response, responsible for the hysteretic behaviour.

In particular, the Yeoh model (Yeoh, 1993) is adopted for the hyperelastic component of the response, whose strain energy potential W has the following expression:

$$W = \sum_{i=1}^3 C_{i0} (I_1 - 3)^i \quad (8)$$

where I_1 is the first invariant of strain tensor and C_{i0} are material parameters.

The Bergstrom-Boyce material model (Bergström and Boyce, 1998) is used to describe the rate-dependent hysteretic behaviour of the rubber. The strain-rate in network B is given by the following equation:

$$\dot{\epsilon}_B = A[\lambda_B - 1]^c (\sigma_B)^m \quad (9)$$

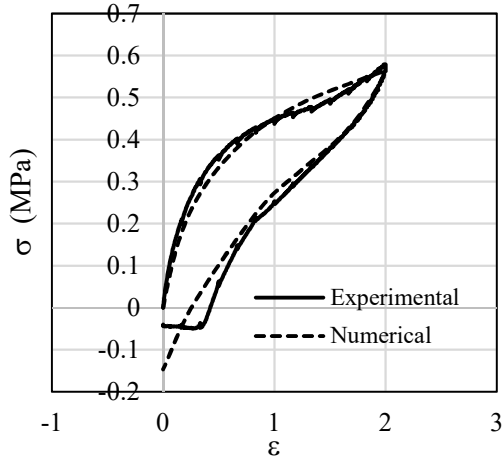
where $\dot{\epsilon}_B$ is the effective creep strain rate, $\lambda_B - 1$ is the nominal creep strain and σ_B is the effective stress. A , m and c are material constants. A stress scaling factor S is also required, which defines the ratio of the stress carried by network B to the stress carried by network A. The total response of the model is obtained by summing the responses of the two networks.

Table 6 shows the values of the parameters of the Yeoh and Bergstrom-Boyce models, which are calibrated to provide the best fit to the tensile tests, and to the shear and the relaxation tests carried out on the quadruplets.

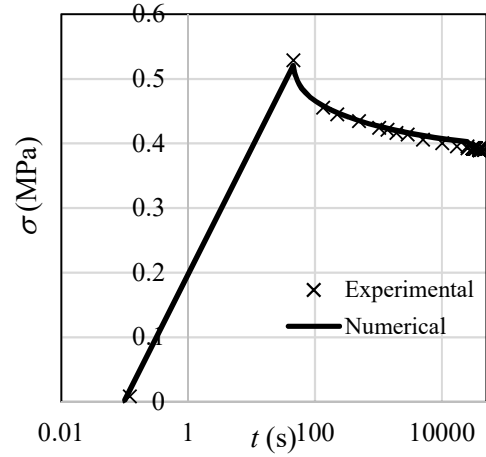
Table 6 Material parameters of Yeoh model (MPa) and Bergstrom-Boyce model

<i>Yeoh model</i>			<i>Bergstrom-Boyce model</i>			
C_{10}	C_{20}	C_{30}	S	A [$S^{-1}MPa^{-1}$]	m	c
0.17	-0.03	0.003	1	0.7	2	-0.5

Figures 28a-b compare the tensile and relaxation tests performed on the tensile rubber sample with the numerical results, whereas Figures 28c-d compare the shear stress-strain response and the relaxation curves of the quadruplet specimen. It can be observed that the proposed model and calibrated parameters provide a very good approximation of the mechanical behaviour of the rubber under different loading conditions.



(a)



(b)

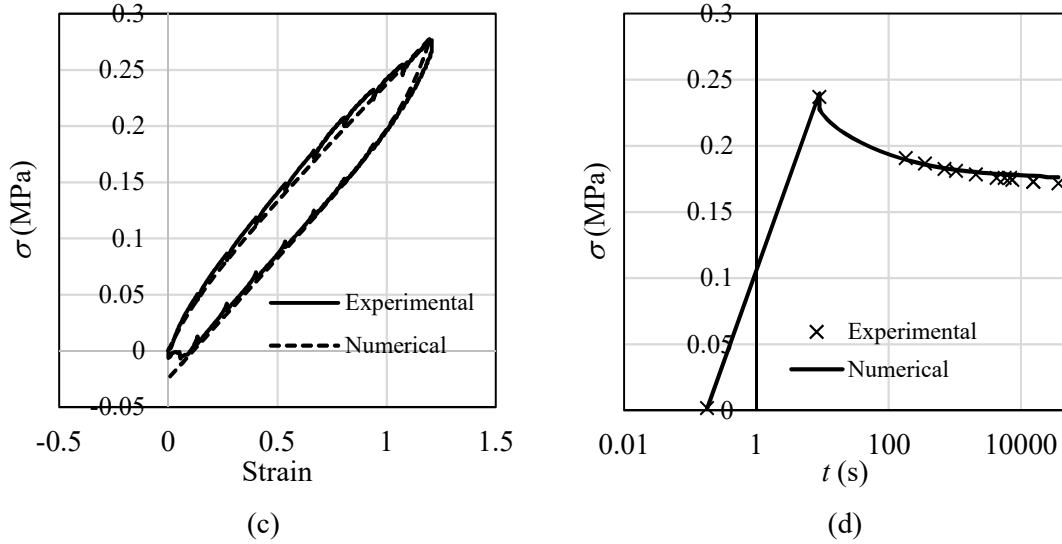


Figure 28. Comparison of experimental and calibrated numerical response of the (a) tensile and (b) relaxation test on tensile rubber sample, (c) shear and (d) relaxation test on quadruplet rubber specimen.

The results of the calibration process show that the Yeoh model combined with Bergstrom-Boyce hysteresis model is a good formulation that can accurately reproduce both tensile and shear tests along with the relaxation tests of the high damping natural rubber material. For this reason, these models are adopted for the simulations of cyclic tests performed on the masonry triplet with rubber joints.

Regarding the triplet numerical model, surface-to-surface contact interfaces are used to simulate the bond between the mortar and rubber layers with interfaces parameter, shown in Table 7, whereas tie constraints have been adopted between the brick-mortar layers since no failures occurred in correspondence of the brick-mortar interfaces during cyclic tests.

Table 7. Properties of the contact interfaces describing the mortar-rubber joints

Mortar Interaction Properties	Mortar-rubber joints
k_n^m per unit area (N/mm ³)	500
k_s^m, k_t^m per unit area (N/mm ³)	250
σ_t (MPa)	0.034
Cohesion, c (MPa)	0.15
Coefficient of friction, μ (-)	0.14
Normal fracture energy per unit area, G_f^I (MPa·mm)	0.005
Shear fracture energy per unit area, G_f^II (MPa·mm)	0.01

Figure 29a shows the model of the masonry triplet with rubber joints. A pressure load has been applied along z direction to simulate the initial pre-compression levels and subsequently three cycles of sinusoidal displacement are applied along the x direction while preventing translation along z and rotation of the external brick blocks. Figure 29b illustrates the deformed shape together with the engineering shear strain distributions of the triplet subjected to the highest pre-compression 0.6 MPa and 20mm lateral displacement. It can be observed that the highest local shear strains are concentrated within the rubber layers. Figures 30-32 show the results of the numerical simulation of cyclic tests under 0.2, 0.4, and 0.6 MPa pre-compression and amplitudes of 10, 15 and 20 mm respectively. A very good agreement can be observed between model predictions and experimental results.

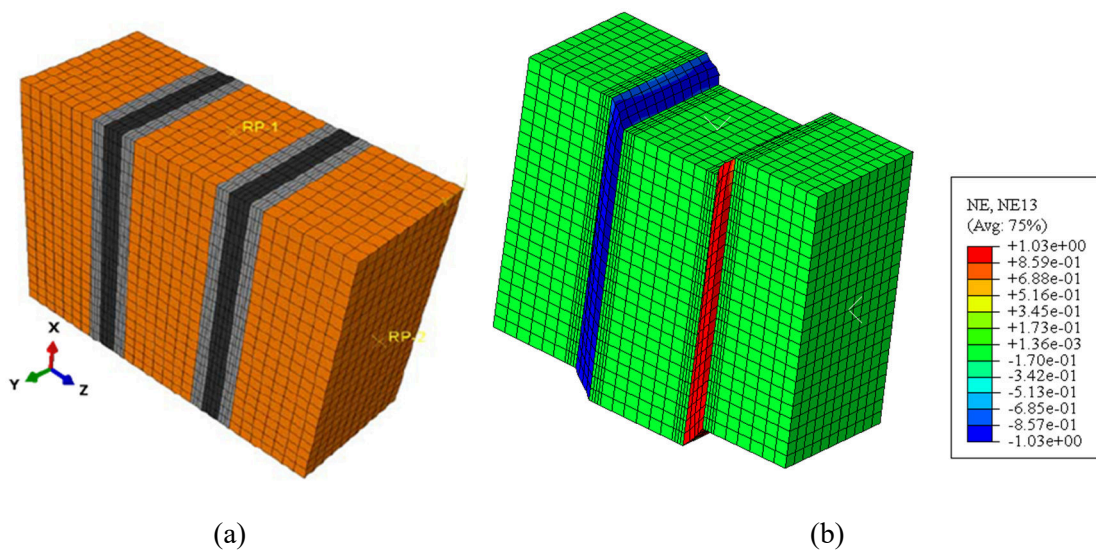


Figure 29. (a) FE model of the masonry triplets with mortar-rubber joints, (b) nominal strain distributions for mortar-rubber triplets subjected to the maximum level of pre-compression in combination with 20 mm lateral displacement

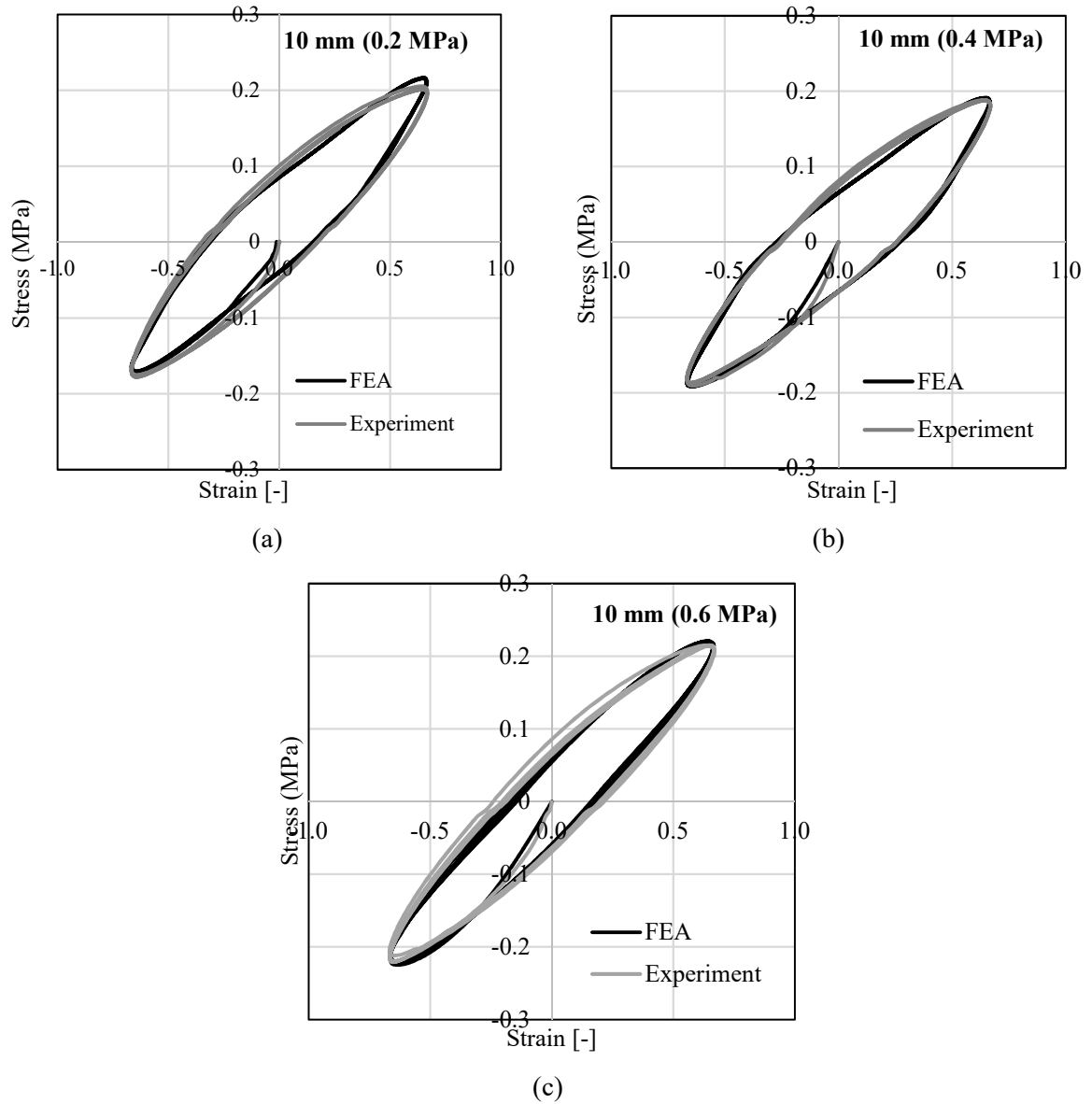


Figure 30. Comparison of experimental and numerical cyclic shear response of the masonry triplet at 10 mm amplitude and pre-compression (a) 0.4 MPa, (b) 0.4 MPa, and (b) 0.6 MPa

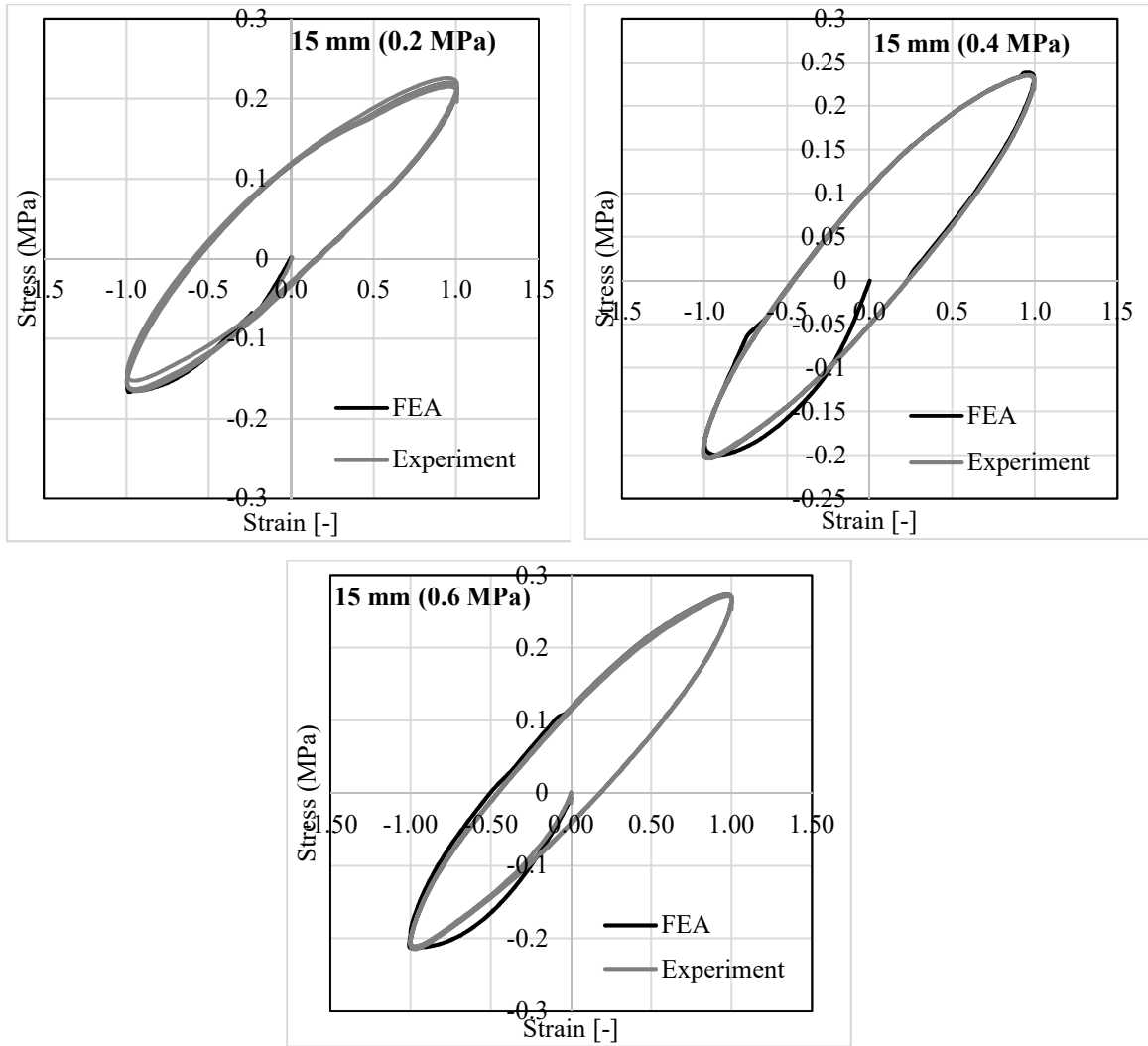
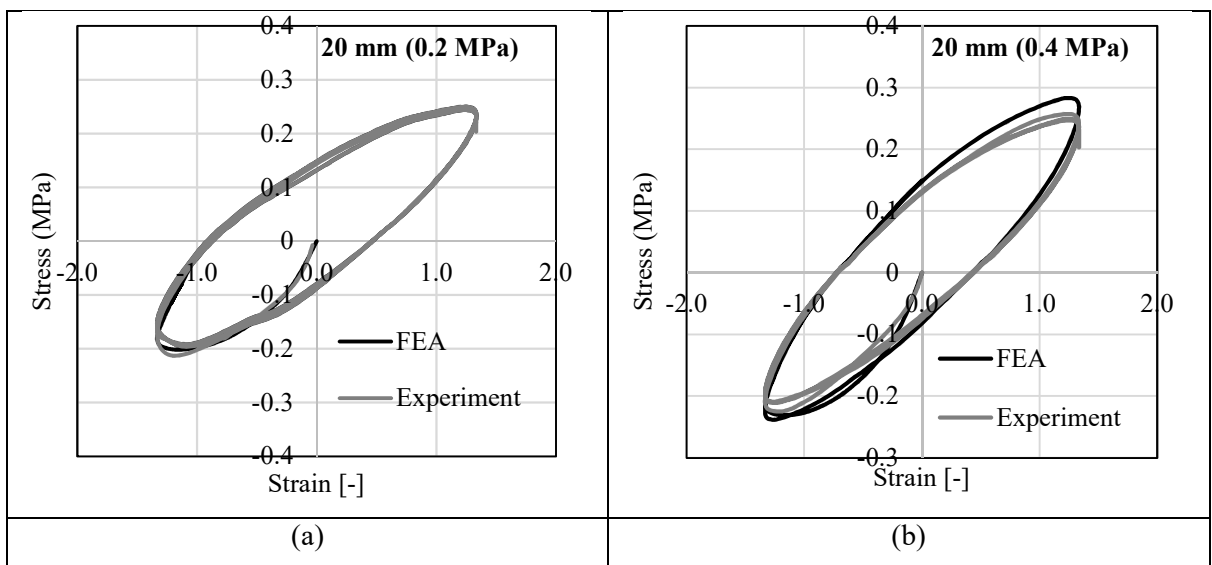


Figure 31 Comparison of experimental and numerical cyclic shear response of the masonry triplet at 10 mm amplitude and pre-compression (a) 0.4 MPa, (b) 0.4 MPa, and (b) 0.6 MPa



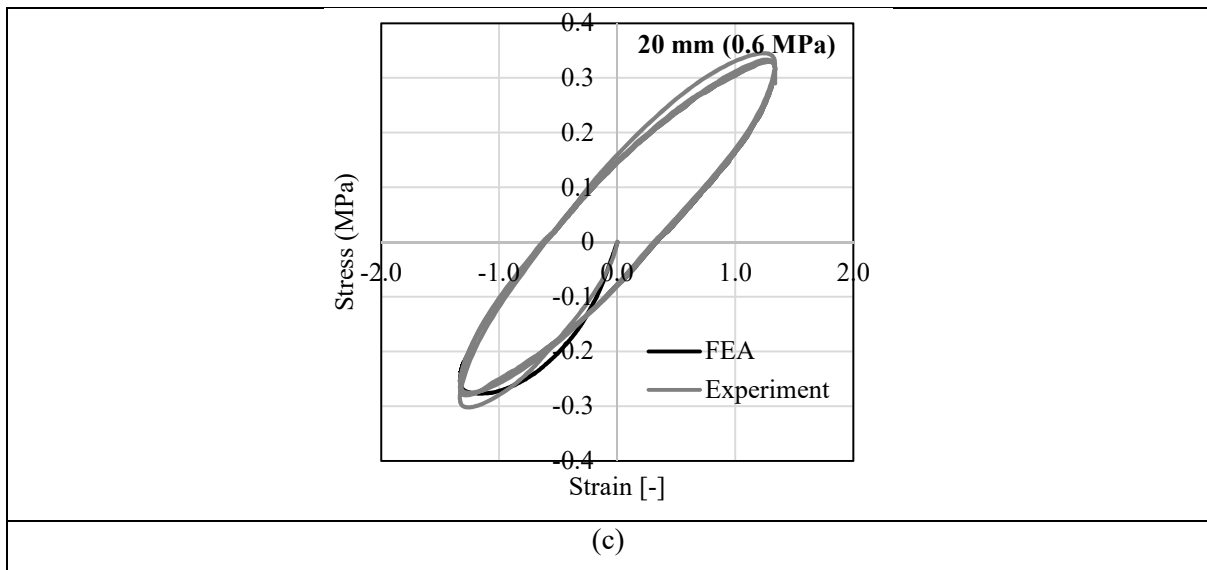


Figure 32. Comparison of experimental and numerical cyclic shear response of the masonry triplet at 20 mm amplitude and pre-compression (a) 0.4 MPa, (b) 0.4 MPa, and (b) 0.6 MPa

4. MODELLING OF RC FRAMES WITH INFILL WALLS AND RUBBER JOINTS

This section describes two modelling strategies that have been developed by the authors for describing the behaviour of RC frames with masonry infill and mortar-rubber joints. The first one is based on an advanced meso-scale modelling of the masonry panels infills with rubber joints, whereas the second one is a more computationally efficient strategy based on the use of macro-elements. Subsections 4.1 and 4.2 illustrate briefly these two modelling strategies, whereas subsection 4.3 shows the results of some studies undertaken to validate them against the results of the quasi-static test carried out on a RC frame with infills and rubber joints within INSYSME project. Finally, Subsection 4.4 describes how the results of the experimental campaign of Section 4.2 can be used to improve these modelling strategies.

4.1. Advanced mesoscale modelling

This modelling strategy is presented in detail in a recent publication by some of the authors of this report (Dhir *et al.*, 2021) and it is only briefly illustrated here. It employs material models and elements already available in a commercial finite element software such as Abaqus (Systèmes, 2016). The RC members of the frame are described with a continuum approach and discretised using 3D 20-noded solid elements, whereas 3D beam elements are used for the reinforcing bars. The concrete behaviour is initially linear elastic, and then it follows the Concrete Damage Plasticity (CDP) model (Lee and Fenves, 1998) once cracking of the concrete in tension or crushing in compression occur. The longitudinal and transverse reinforcement are rigidly embedded within the concrete through the “embedded element technique” (Systèmes, 2016).

The mortar joints and rubber-mortar interface properties are described in a simplified way using surface-to-surface contact interfaces. In general, the surface-to-surface interaction is described by a linear elastic traction separation relationship for the condition prior to damage. Assuming uncoupled behaviour, this is controlled by the stiffness along the direction normal to the joint, k_n , and along two orthogonal shear directions in the plane of the joint, k_s and k_t . The values of the joint stiffnesses depend on the elastic properties of the components and on the geometry of the joints (Lourenço, 1997).

The mortar-rubber-mortar joints work, from a mechanical point of view, as a series system. Thus, the composite stiffness of a mortar-rubber-mortar joint in the normal and the two, in plane and out-of-plane, shear directions can be approximated as follows:

$$\frac{1}{k_i^{mr}} = \frac{1}{k_i^r} + \frac{2}{k_i^m} \quad i = n, s, t \quad (5)$$

where r and m denotes rubber and mortar respectively.

The values of k_s^{mr} are controlled by the compliance of the rubber, which is much higher than that of the mortar in order to accommodate large displacements of the in-plane motion of the frame and the wall. The rubber stiffness as $k_s^r = G_r / t_r$, where $G_r = 0.50$ Mpa and $t_r = 15$ mm for the joints.

With regards to the maximum allowable stresses in the mortar-rubber joints, under the series system approximation they can be assumed to coincide with the lowest among the values of the strengths of the constitutive components and the values of the bond resistance. The experimental tests of Section 2 have shown that the mortar layer-brick bond and the mortar layer-rubber layer bond are the weakest component for the investigated systems.

4.2. Simplified macro-scale model

This modelling strategy is based on the use of 2D macro-elements, originally developed by Calio' and Panto' (Caliò and Pantò, 2014), subsequently implemented in OpenSees (Mazzoni *et al.*, 2006) by Panto' and Rossi (Pantò and Rossi, 2019). Figure 33a illustrates a masonry-infilled frame where the horizontal joints divide the infill into a series of subpanels, which are surrounded by flexible/sliding joints. Figure 33b illustrates the mechanical scheme of a macro-element, which consists of an articulated quadrilateral (the panel), a one-dimensional (1D) diagonal link, and eight two-dimensional (2D) zero-length links. According to the simplified formulation developed in (Pantò and Rossi, 2019), the two 2D links placed on each rigid element of the panel are used to

connect the macro-element to the adjacent macro-elements, to beam/column elements, or to external supports. Rigid offsets allow for a geometrically consistent simulation of the interaction between the infill and the beam/column external face. The kinematics of each macro-element is described by 20 degrees of freedom, 16 associated with the normal and shear displacements of the perimeter nodes connecting the 2D links and 4 degrees of freedom associated with the kinematics of the internal panel describing the in-plane rigid motion plus the panel shear deformation.

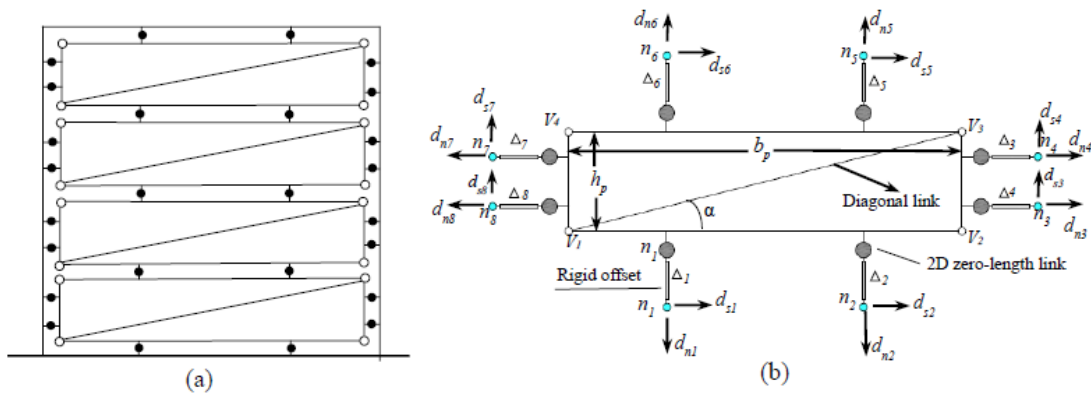


Figure 33. (a) Infilled frame with horizontal and vertical flexible/sliding joints and (b) mechanical scheme of a macro-element

A detailed analytical formulation of the macro-element and the calibration of the model parameters for the case of traditional masonry infills is available in (Pantò and Rossi, 2019). The same macro-element can also be used to describe a subpanel surrounded by rubber. In particular, tensile/compression behaviour of the masonry subpanels and of the flexible joints is simulated through the normal response of the 2D contact links, sliding of the low-friction joints and shear deformations of the rubber joints are simulated through the tangential response of the 2D contact links, and diagonal shear behaviour of the masonry subpanels is simulated by the diagonal links.

4.3. Case study validation

A calibration/validation study of the two modeling approaches is conducted by considering the experimental tests performed within INSYSME project (EU Project INSYSME, 2016) on a RC frame with masonry infills and mortar-rubber joints (DRES-V2). The infill panels are made with hollow clay masonry blocks (D-type) arranged in a running bond pattern (Figure 34). The bed joints are fully filled with mortar and they are 10 mm thick, whereas there are no mortar head joints and the transfer of stresses from a brick to the adjacent ones relies on the brick interlocking. Some details regarding the frame, including the frame cross sections, rebar diameter and detailing scheme and masonry block dimensions, are given in Figure 34. Further details are available in Verlato (Verlato, 2017). The experimental quasi-static tests consisted of the application of vertical loads (200 kN) at the top of each column, simulating the effect of permanent loads acting on the frame, followed by

in-plane horizontal loads (monotonically increasing) applied at the beam extreme, as shown in Figure 34.

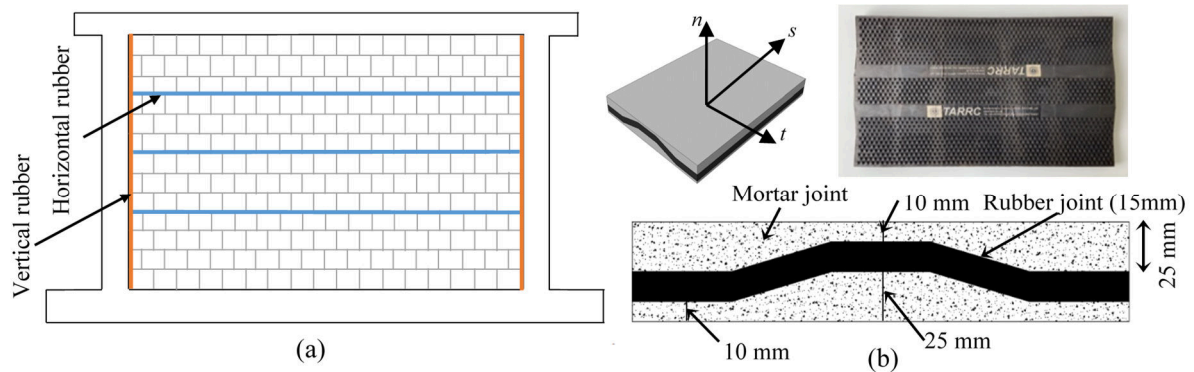


Figure 34 Geometric details of the frame with traditional infill (dimensions in mm)

Table 8. Main mechanical properties of RC components and selected masonry infill. Table 8 reports the main mechanical properties of the concrete and steel reinforcement employed for the frame components, the brick and the masonry infill. Table 9 reports the properties of the interfaces describing the mortar joints in the meso-scale model. The values in Table 8 and Table 9 are based on the results of the experimental tests carried out by INSYSME (EU Project INSYSME, 2016) and numerical models developed by Verlato (Verlato, 2017) to simulate these tests. The head joints have been given different properties to account for the fact that they were not filled with mortar.

Table 8. Main mechanical properties of RC components and selected masonry infill.

Mechanical properties	Concrete	Steel reinforcement	Brick units		Masonry infill	
			Parallel to holes	Perpendicular to holes	Vertical	Horizontal
Elasticity modulus E (MPa)	22000	180000	7147	3693	6158	1904
Poisson Ratio ν (-)	0.15	0.3	-	-	0.4	0.4
Compressive strength f_c (MPa)	40	-	12900	4250	7.63	1.40
Yield strength (MPa)	-	535	-	-	-	-
Tensile strength f_t (MPa)	3.9	-	0.33	0.22	0.52	0.1
Post-elastic to elastic stiffness ratio	-	0.002	-	-	-	-

Table 9. Properties of the contact interfaces describing the mortar joints

Mortar Interaction Properties	Bed joints	Head joints
k_n^m per unit area (N/mm ³)	200	200
k_s^m, k_t^m per unit area (N/mm ³)	100	-
Tensile strength f_t (MPa)	0.346	-
Cohesion c (MPa)	0.485	-
Friction coefficient μ (-)	1.13	0.8
Fracture energy in tension G_f^I (MPa·mm)	0.005	-
Fracture energy in shear G_f^{II} (MPa·mm)	0.05	-

Table 10 reports the values of the mechanical parameters describing the horizontal mortar-rubber joints and the vertical rubber joints at the interface between the infill and the frame in the 3D mesoscale model. The value assumed for the mortar layer stiffness does not affect significantly the composite joint properties, which are controlled by the rubber layer compliance. It is noteworthy that the description of the shear behaviour of the 2D links in the model with macro-elements follows the same approach as that of the meso-scale model, whereas the normal behaviour accounts for the behaviour of both the tributary panel area and of the joint (forming a series mechanical system).

Table 10. Interaction properties of the mortar-rubber joints in the mesoscale model.

Interaction properties	Horizontal layer	Vertical layer
k_n^{mr} per unit area (N/mm ³)	11.7	1
k_s^{mr}, k_t^{mr} per unit area (N/mm ³)	0.033	0
f_t (MPa)	0.15	0
c (MPa)	0.05	0
μ (-)	0.36	0.31
G_f^I (MPa·mm)	0.005	-
G_f^{II} (MPa·mm)	0.04	-

Figure 35a shows the minimum (most compressive) principal stress distribution at 2% inter-storey drift obtained using the more advanced 3D modelling approach. Overall, it can be observed that most of the deformation in the infill is localized in correspondence of the rubber joints. Some cracks are observed at the top left corner of the lower portion of the wall, just below the first rubber layer. Other cracks are found on the right side of the top three subpanels. It is noteworthy that all

these cracks were also observed experimentally (Verlato, 2017). Figure 35b shows the plastic strain distribution indicating the cracking of the bricks under 2% inter-storey drift. Figure 35c shows the deformed shape obtained with the simplified modelling approach, which features the sliding between the subpanels in correspondence of the horizontal rubber joints, and diagonal struts forming in each subpanel.

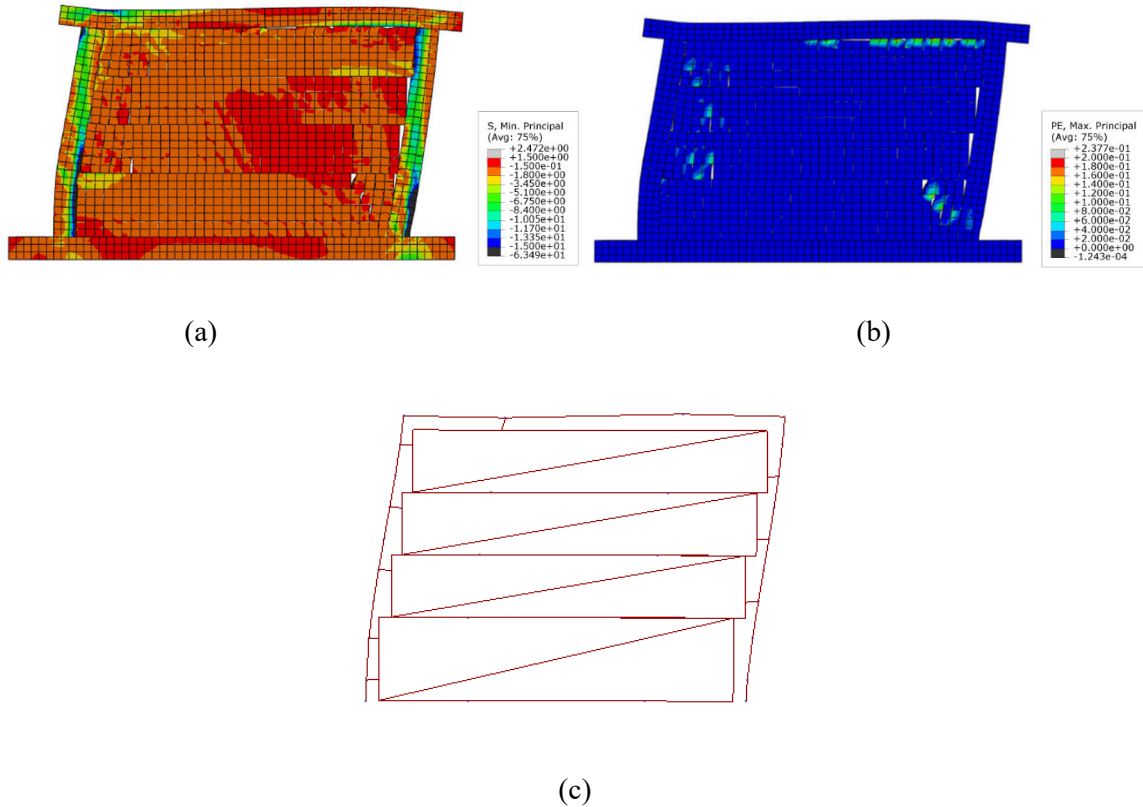


Figure 35 (a) Minimum principal compressive stress distribution (b) Plastic strain contour plots for infilled frame with rubber joints (c) Deformed shape of the DMEM for a horizontal displacement of 55mm (2.0% drift)

Figure 36 shows the force-displacement curves of the system with rubber joints according to the experimental tests and the numerical simulations using the two different models. Both the numerical approaches adopted in the present study provide accurate estimates of the response, with a global force-deflection curve very close to the experimental one. However, the 3-D model (12812 nodes) requires 85 hrs to reach a displacement of 93 mm, compared to 24 seconds required by the other more computationally efficient model (with only 30 nodes).

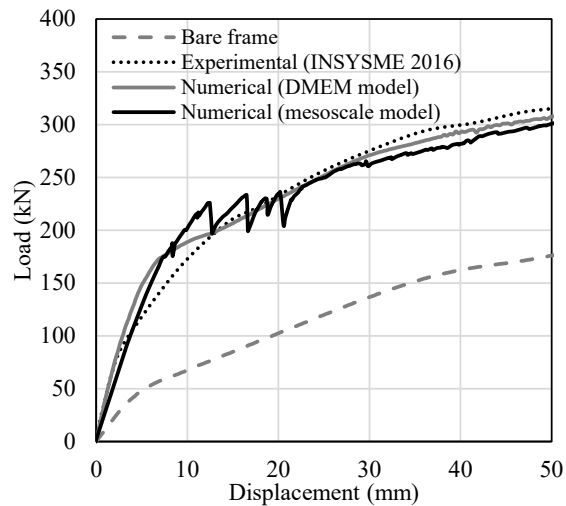


Figure 36. Comparison between numerical responses of the bare frame, infilled frame with traditional infills and infill with rubber joints under monotonic loading.

4.4. Model developments

The modelling strategies developed thus far and described in the previous subsections are able to simulate with good accuracy the quasi-static response of RC frames with rubber joints under in-plane loading. However, they cannot be employed for evaluating the dynamic behaviour of these systems, and thus they are not suitable for seismic performance assessment purposes, due to the limitations inherent to the interface models describing the rubber-mortar joints. In fact, the interface models, which are very similar in both the modelling strategies, need to be extended in order to simulate the energy dissipation capabilities of the rubber joints, as also emerged during the tests described in Section 2. A simple way to account for this would be to replace the linear elastic behaviour of the model with a visco-elastic one, calibrated to fit available experimental results. Alternatively, a more sophisticated rubber model could be employed, e.g. using the one developed by (Tubaldi *et al.*, 2017) and accounting for many important features of the shear behaviour of high-damping rubber compounds. Implementing these models would unlock the capabilities of the proposed modelling strategies to describe the dynamic response of infilled RC frames with rubber joints, and thus to evaluate the contribution of the rubber joints to the overall damping capacity of the system. Based on some preliminary analysis results illustrated in (Verlato, 2017), relatively high values of damping capacities could be achieved, which could be helpful for improving the seismic performance of masonry-infilled frames and reducing their seismic vulnerability and risk. Thus, the rubber joints would help to turn the infills from a critical component in RC frames into a beneficial one.

5. CONCLUDING REMARKS

This report has presented the outcomes of an experimental campaign and numerical simulations aimed at characterizing the mechanical behaviour of mortar-rubber joints, and particularly their dissipation capacity. These joints can be employed for improving the seismic performance of masonry-infilled reinforced-concrete (RC) frame structures, by increasing the flexibility of infill panels and isolating them from the surrounding frames. The rubber joints are also expected to provide an additional source of energy dissipation, thanks to the use of a high-damping rubber compound, although this has not been fully demonstrated by past experimental tests, which considered only quasi-static loading conditions. In order to fill this gap, a shear test set-up has been developed at University of Strathclyde in order to test masonry triplets with mortar-rubber joints under cyclic loading.

The study results have shown that the rubber compound developed by TARRC exhibits good dissipative properties. However, in order to exploit this, particular care must be placed in the design and manufacturing stage, in order to ensure good bond properties between the rubber layers and the mortar layers, which is the weakest component of the composite system. The rubber layers should be designed to undergo shear deformations below the bond capacity.

Together with the experimental test results, the numerical simulations of the tests with a micro-modelling approach are described. Moreover, two alternative modelling strategies for simulating the behaviour of RC frames with infills and rubber joints are briefly illustrated, by also outlining the extensions required in order to use them to describe the dynamic behaviour and seismic response of the system.

The proposed devices are expected to improve the resilience of reinforced concrete structures under seismic hazard, helping to minimize human losses, building downtime, repair costs, and facilitating the evacuation of people from buildings during strong earthquakes, thanks to the reduction of the seismic damage of one of the most critical components of RC frames. The results of this report provide a contribution towards the diffusion of this technology, which can be particularly useful for developing countries, due to its cost effectiveness and ease of installation.

Acknowledgments

The support of Earthquake Engineering Field Investigation Team (EEFIT) and the Institution of Structural Engineers, through the 2019 EEFIT Research Grant Scheme, is gratefully acknowledged.

References

Ahmadi, H., Dusi, A. and J. Gough. (2017) 'A Rubber-Based System for Damage Reduction in Infill Masonry Walls', in *16th World Conference on Earthquake Engineering, 16WCEE*.

Anglada, X. R. (2014) *Shear tests on masonry triplets with different soft layer membranes*. Swiss Federal Institute of Technology, Zürich.

Barattucci, S. *et al.* (2020) 'An experimental and numerical study on masonry triplets subjected to monotonic and cyclic shear loadings', *Construction and Building Materials*, 254, p. 119313. doi: 10.1016/j.conbuildmat.2020.119313.

Bergström, J. S. and Boyce, M. C. (1998) 'Constitutive modeling of the large strain time-dependent behavior of elastomers', *Journal of the Mechanics and Physics of Solids*, 46(5), pp. 931–954. doi: 10.1016/S0022-5096(97)00075-6.

Bolis, V. *et al.* (2015) 'In-plane behaviour of innovative masonry infills based on different configurations of wooden sliding joints', *Earthquake Resistant Engineering Structures X*, 1, pp. 289–301. doi: 10.2495/eres150241.

Bolis, V. *et al.* (2019) 'Numerical Investigation of the In-Plane Performance of Masonry-Infilled RC Frames with Sliding Subpanels', *Journal of Earthquake Engineering*, 5(2), pp. 792–817. doi: 10.1002/eqe.3163.

Bolis, V., Stavridis, A. and Preti, M. (2017) 'Numerical Investigation of the In-Plane Performance of Masonry-Infilled RC Frames with Sliding Subpanels', *Journal of Structural Engineering (United States)*, 143(2), pp. 1–18. doi: 10.1061/(ASCE)ST.1943-541X.0001651.

Calabria, A. *et al.* (2016) 'Innovative systems for masonry infill walls based on the use of rubber joints: Finite element modelling and comparison with in-plane tests', *Brick and Block Masonry: Trends, Innovations and Challenges - Proceedings of the 16th International Brick and Block Masonry Conference, IBMAC 2016*, pp. 1155–1162. doi: 10.1201/b21889-144.

Caliò, I., Marletta, M. and Pantò, B. (2012) 'A new discrete element model for the evaluation of the seismic behaviour of unreinforced masonry buildings', *Engineering Structures*, 40, pp. 327–338. doi: 10.1016/j.engstruct.2012.02.039.

Caliò, I. and Pantò, B. (2014) 'A macro-element modelling approach of Infilled Frame Structures', *Computers and Structures*, 143, pp. 91–107. doi: 10.1016/j.compstruc.2014.07.008.

Concrete damaged plasticity (2017) *Abaqus manual*. Available at: <https://abaqus-docs.mit.edu/2017/English/SIMACAEMATRefMap/simamat-c-concretedamaged.htm>.

- Dhir, P. K. *et al.* (2021) ‘Numerical modelling of reinforced concrete frames with masonry infill and rubber joints’, *Engineering Structures*, 246(July), p. 112833. doi: 10.1016/j.engstruct.2021.112833.
- Dolatshahi, K. M. and Aref, A. J. (2011) ‘Two-dimensional computational framework of meso-scale rigid and line interface elements for masonry structures’, *Engineering Structures*, 33(12), pp. 3657–3667. doi: 10.1016/j.engstruct.2011.07.030.
- El-Dakhkhni, W. W., Drysdale, R. G. and Khattab, M. M. (2006) ‘Multilaminate macromodel for concrete masonry: formulation and verification’, *Journal of Structural Engineering*, 132(12), pp. 1984–1996. doi: 10.1061/(ASCE)0733-9445(2006)132:12(1984).
- EN 1015-11 (2006) ‘Methods of Test for Mortar for Masonry’, *Part 11: Determination of Flexural and Compressive Strength of Hardened Mortar*, 3(1).
- EN 1052-3 (2002) ‘Methods of Test for Mortar for Masonry’, *Part 3: Determination of initial shear strength*, 3(1).
- EU Project INSYSME (2016) *INnovative SYStems for earthquake resistant Masonry Enclosures in reinforced concrete buildings*, FP7-SME-2013-2- GA606229GA606229. Available at: www.insysme.eu.
- Filiatrault, A. and Sullivan, T. (2014) ‘Performance-based seismic design of nonstructural building components: The next frontier of earthquake engineering’, *Earthquake Engineering and Engineering Vibration*, 13(1), pp. 17–46. doi: 10.1007/s11803-014-0238-9.
- Lee, J. and Fenves, G. L. (1998) ‘A plastic-damage concrete model for earthquake analysis of dams’, *Earthquake Engineering and Structural Dynamics*, 27(9), pp. 937–956. doi: 10.1002/(SICI)1096-9845(199809)27:9<937::AID-EQE764>3.0.CO;2-5.
- Lourenço, P. B. and Rots, J. G. (1997) ‘Multisurface interface model for analysis of masonry structures’, *Journal of Engineering Mechanics*, 123(7), pp. 660–668. doi: 10.1061/(ASCE)0733-9399(1997)123:7(660).
- Lourenço, P. J. B. B. (1997) *Computational strategies for masonry structures*. Doctoral dissertation, Delft University of Technology, Holland. Available at: <http://www.narcis.nl/publication/RecordID/oai:tudelft.nl:uuid:4f5a2c6c-d5b7-4043-9d06-8c0b7b9f1f6f>.
- Macorini, L. and Izzuddin, B. (2011) ‘A non-linear interface element for 3D mesoscale analysis of brick-masonry structures’, *International Journal for numerical methods in Engineering*, 85(12),

pp. 1584–1608.

Macorini, L. and Izzuddin, B. A. (2013) ‘Nonlinear analysis of masonry structures using mesoscale partitioned modelling’, *Advances in Engineering Software*, 60–61, pp. 58–69. doi: 10.1016/j.advengsoft.2012.11.008.

Macorini, L. and Izzuddin, B. A. (2014) ‘Nonlinear analysis of unreinforced masonry walls under blast loading using Mesoscale partitioned modeling’, *Journal of structural engineering*, 140(8), pp. 1–10. doi: 10.1061/(ASCE)ST.1943-541X.0000931.

Mazzoni, S. *et al.* (2006) ‘Open System for Earthquake Engineering Simulation (OpenSEES) user command-language manual’, *Pacific Earthquake Engineering Research Center*, p. 465.

Misir, I. S. (2015) ‘Potential Use of Locked Brick Infill Walls to Decrease Soft-Story Formation in Frame Buildings’, *Journal of Performance of Constructed Facilities*, 29(5), p. 04014133. doi: 10.1061/(asce)cf.1943-5509.0000633.

Mojsilović, N. (2012) ‘Masonry elements with damp-proof course membrane: Assessment of shear strength parameters’, *Construction and Building Materials*, 35, pp. 1002–1012. doi: 10.1016/j.conbuildmat.2012.04.033.

Mojsilović, N., Petrović, M. and Anglada, X. R. (2015) ‘Masonry elements with multi-layer bed joints: Behaviour under monotonic and static-cyclic shear’, *Construction and Building Materials*, 100, pp. 149–162.

Mojsilović, N., Petrović, M. and Anglada, X. R. (2015) ‘Masonry elements with multi-layer bed joints: Behaviour under monotonic and static-cyclic shear’, *Construction and Building Materials*, 100, pp. 149–162. doi: 10.1016/j.conbuildmat.2015.09.065.

Mojsilović, N., Petrović, M. and Stojadinović, B. (2019) ‘Multi-layer masonry bed joint subjected to shear: Analytical modelling’, *Construction and Building Materials*, 205, pp. 602–610. doi: 10.1016/j.conbuildmat.2019.02.051.

Morandi, P. *et al.* (2017) ‘Experimental Tests of an Engineered Seismic Solution of Masonry Infills With Sliding Joints’, 4442(Abstract ID).

Morandi, P., Milanesi, R. R. and Mageses, G. (2016) ‘Innovative seismic solution for clay masonry infills with sliding joints: Principles and details’, *Brick and Block Masonry: Trends, Innovations and Challenges - Proceedings of the 16th International Brick and Block Masonry Conference, IBMAC 2016*, pp. 1273–1282. doi: 10.1201/b21889-158.

Morandi, P., Milanesi, R. R. and Mageses, G. (2018) ‘Innovative solution for seismic-resistant

- masonry infills with sliding joints: in-plane experimental performance', *Engineering Structures*, 176(September), pp. 719–733. doi: 10.1016/j.engstruct.2018.09.018.
- Nasiri, E. and Liu, Y. (2017) 'Development of a detailed 3D FE model for analysis of the in-plane behaviour of masonry infilled concrete frames', *Engineering Structures*, 143, pp. 603–616. doi: 10.1016/j.engstruct.2017.04.049.
- Nicoletti, V. *et al.* (2020) 'Expeditious methodology for the estimation of infill masonry wall stiffness through in-situ dynamic tests', *Construction and Building Materials*, 262, p. 120807. doi: 10.1016/j.conbuildmat.2020.120807.
- Pantò, B., Calì, I. and Lourenço, P. J. B. B. (2017) 'Seismic safety evaluation of reinforced concrete masonry infilled frames using macro modelling approach', *Bulletin of Earthquake Engineering*, 15(9), pp. 3871–3895. doi: 10.1007/s10518-017-0120-z.
- Pantò, B. and Rossi, P. P. (2019) 'A new macromodel for the assessment of the seismic response of infilled RC frames', *Earthquake Engineering and Structural Dynamics*, 48(7), pp. 792–817. doi: 10.1002/eqe.3163.
- Petrović, M., Stojadinović, B. and Mojsilović, N. (2017) 'I-Shaped Unreinforced Masonry Wallettes with a Soft-Layer Bed Joint: Behavior under Static-Cyclic Shear', *Journal of structural engineering*, 143(11), pp. 1–20. doi: 10.1061/(ASCE)ST.1943-541X.0001884.
- Pietruszczak, S. and Niu, X. (1992) 'A mathematical description of macroscopic behaviour of brick masonry', *International Journal of Solids and Structures*, 29(5), pp. 531–546. doi: 10.1016/0020-7683(92)90052-U.
- Preti, M. *et al.* (2016) 'Analysis of the in-plane response of earthen masonry infill panels partitioned by sliding joints', *Earthquake Engineering & Structural Dynamics*, 45(8), pp. 1209–1232.
- Preti, M., Bettini, N. and Plizzari, G. (2007) 'Infill walls with sliding joints to limit infill-frame seismic interaction: large-scale experimental test', *Pacific Conference on Earthquake Engineering*, (056), pp. 1–6. doi: 10.1002/eqe.
- Preti, M., Bettini, N. and Plizzari, G. (2012) 'Infill walls with sliding joints to limit infill-frame seismic interaction: Large-scale experimental test', *Journal of Earthquake Engineering*, 16(1), pp. 125–141. doi: 10.1080/13632469.2011.579815.
- Preti, M., Bolis, V. and Stavridis, A. (2019) 'Seismic infill–frame interaction of masonry walls partitioned with horizontal sliding joints: analysis and simplified modeling', *Journal of*

Earthquake Engineering, 23(10), pp. 1651–1677. doi: 10.1080/13632469.2017.1387195.

Preti, M., Migliorati, L. and Giuriani, E. (2015) ‘Experimental testing of engineered masonry infill walls for post-earthquake structural damage control’, *Bulletin of Earthquake Engineering*, 13(7), pp. 2029–2049. doi: 10.1007/s10518-014-9701-2.

De Risi, M. T., Del Gaudio, C. and Verderame, G. M. (2019) ‘Evaluation of repair costs for masonry infills in RC buildings from observed damage data: The case-study of the 2009 L’Aquila earthquake’, *Buildings*, 9(5). doi: 10.3390/buildings9050122.

Rots, J. G. (1997) *Structural masonry: An experimental/numerical basis for practical design rules*. TNO Building and Construction Research, Rijswijk, Netherlands: Centre of Civil Engineering Research and Codes (CUR).

Ruggieri, S. *et al.* (2021) ‘Two frugal options to assess class fragility and seismic safety for low-rise reinforced concrete school buildings in Southern Italy’, *Bulletin of Earthquake Engineering*, 19(3), pp. 1415–1439. doi: 10.1007/s10518-020-01033-5.

Ruggieri, S., Porco, F. and Uva, G. (2020) *A practical approach for estimating the floor deformability in existing RC buildings: evaluation of the effects in the structural response and seismic fragility*, *Bulletin of Earthquake Engineering*. Springer Netherlands. doi: 10.1007/s10518-019-00774-2.

SAIE (2015) *SAIE*. Available at: <http://www.saie.bolognafiere.it/en/>.

Sarhosis, V., Tsavdaridis, K. D. and Giannopoulos, I. (2014) ‘Discrete Element Modelling of Masonry Infilled Steel Frames with Multiple Window Openings Subjected to Lateral Load Variations’, *The Open Construction and Building Technology Journal*, 8(1), pp. 93–103. doi: 10.2174/1874836801408010093.

Singh, S. B., Munjal, P. and Thammishetti, N. (2015) ‘Role of water/cement ratio on strength development of cement mortar’, *Journal of Building Engineering*, 4, pp. 94–100. doi: 10.1016/j.jobbe.2015.09.003.

Sutcliffe, D. J., Yu, H. S. and Page, A. W. (1999) ‘Lower bound limit analysis of unreinforced masonry shear walls’, *Numerical models in geomechanics. Proceedings of the 7th international symposium, Graz, September 1999.*, 79, pp. 639–644. doi: 10.1201/9781003078548-110.

Systèmes, D. (2016) *Abaqus, RI: Dassault Systèmes*. Available at: <http://www.3ds.com/products-services/simulia/products/abaqus/>.

Di Trapani, F. *et al.* (2020) ‘Seismic reliability and loss assessment of RC frame structures with

traditional and innovative masonry infills', *Engineering Structures*, 208(February), p. 110306. doi: 10.1016/j.engstruct.2020.110306.

Tubaldi, E. *et al.* (2017) 'Stress softening behaviour of HDNR bearings: modelling and influence on the seismic response of isolated structures', *Earthquake Engineering & Structural Dynamics*, 46(12), pp. 2033–2054. doi: 10.1002/eqe.

Uva, G. *et al.* (2012) 'On the role of equivalent strut models in the seismic assessment of infilled RC buildings', *Engineering Structures*, 42, pp. 83–94. doi: 10.1016/j.engstruct.2012.04.005.

Del Vecchio, C. *et al.* (2018) 'Repair costs of existing rc buildings damaged by the l'aquila earthquake and comparison with FEMA P-58 predictions', *Earthquake Spectra*, 34(1), pp. 237–263. doi: 10.1193/122916EQS257M.

Verlato, N. *et al.* (2016) 'Innovative systems for masonry infill walls based on the use of deformable joints: Combined in-plane/out-of-plane tests', *Brick and Block Masonry: Trends, Innovations and Challenges - Proceedings of the 16th International Brick and Block Masonry Conference, IBMAC 2016*, pp. 1359–1366. doi: 10.1201/b21889-168.

Verlato, N. (2017) *Development of a Clay Masonry Enclosure System With Deformable Joints : Experimental Analysis and Numerical*. Doctoral dissertation, Università Degli Studi Di Brescia, Italy.

Villaverde, R. (1997) 'Seismic design of secondary structures: state of the art', *Journal of structural engineering*, 123(8), pp. 1011–1019. doi: 10.1061/(ASCE)0733-9445(1997)123:8(1011).

Vögeli, C., Mojsilović, N. and Stojadinović, B. (2015) 'Masonry wallettes with a soft layer bed joint: Behaviour under static-cyclic loading', *Engineering Structures*, 86, pp. 16–32. doi: 10.1016/j.engstruct.2014.12.038.

Yeoh, O. (1993) 'Some Forms of the Strain Energy Function for Rubber', *Rubber Chemistry and Technology*, 66, 754–77, pp. 66, 754–771. doi: 10.1080/00033799300200371.